# LIDAR INVESTIGATIONS OF SNOW DISTRIBUTION IN MOUNTAINOUS TERRAIN

by

Alden Taylor Shallcross

A thesis

submitted in partial fulfillment

of the requirements for the degree of

Master of Science in Hydrologic Sciences

Boise State University

May 2012

BOISE STATE UNIVERSITY GRADUATE COLLEGE

# DEFENSE COMMITTEE AND FINAL READING APPROVALS

of the thesis submitted by

Alden Taylor Shallcross

Thesis Title: LiDAR Investigations of Snow Distribution in Mountainous Terrain

Date of Final Oral Examination: 21 October 2011

The following individuals read and discussed the thesis submitted by student Alden Taylor Shallcross, and they evaluated his presentation and response to questions during the final oral examination. They found that the student passed the final oral examination.

| | |
|---|---|
| James P. McNamara, Ph.D. | Chair, Supervisory Committee |
| Alejandro M. Flores, Ph.D. | Member, Supervisory Committee |
| Hans Peter Marshall, Ph.D. | Member, Supervisory Committee |

The final reading approval of the thesis was granted by James P. McNamara, Ph.D., Chair of the Supervisory Committee. The thesis was approved for the Graduate College by John R. Pelton, Ph.D., Dean of the Graduate College.

ACKNOWLEDGEMENTS

I would like to thank those who helped make this work possible. Thank you, Dr. James McNamara, my advisor, for providing me with this opportunity. He was always willing to assist and was a flexible leader, empowering me to explore the many areas of this research. Thank you to my committee: Dr. Hans-Peter Marshall, whose snow science and programming expertise was crucial in this study. He always made time to entertain my ideas and helped me work through the numerous programming challenges that were intrinsically tied to a study of this nature. I sincerely appreciate all of Dr. Nancy Glen's remote sensing guidance and willingness to support my research. She selflessly offered up her time and resources. Thank you, Dr. Alejandro Flores, for all of your programming assistance. Thanks to Lucas Spaete and Rupesh Shrestha, who were always willing to collaborate with me to solve complex LiDAR processing issues.

I could not have collected the ground validation datasets, crucial to this study, without the field assistance from Patrick Kormos, Dave Eiriksson, Erik Boe, Alison Burnop, Brian Anderson, and others.

Funding was provided from the National Oceanic and Atmospheric Administration - National Weather Service and the Boise State Geosciences Department.

## ABSTRACT

An algorithm is constructed to use snow-depth estimates, derived from repeat airborne LiDAR (Light Detection and Ranging), to identify the sampling strategy that requires the fewest total measurements to estimate the total snow volume in the Dry Creek Experimental Watershed (DCEW) Idaho. LiDAR is used to map snow cover by differencing the digital elevation models (DEMs) obtained from a snow-covered overflight and a snow-free overflight. Sixteen independent variables known to influence snow distribution are derived from a LiDAR digital elevation dataset, obtained during snow-free conditions, and used to predict snow distribution via binary regression trees. Variable ranges leading to the terminal nodes are used to segment the watershed. The algorithm calculates the minimum total number of samples needed to meet pre-defined accuracy thresholds for estimating total basin snow volume. It uses an iterative process to incrementally assign depth measurements to the region that maximizes the reduction in the mean absolute deviation (MAD) of snow volume. It identifies the best combination of regions by constraining the size of the terminal nodes in the binary regression tree and repeating the sampling code for each set of discrete regions. The combination of regions that requires the fewest samples to achieve the desired level of accuracy is suggested for use. Thus, during future field campaigns, an optimal number of point measurements of snow depth can be gathered, averaged, and distributed throughout each region. Each unit's snow volume can then be summed to estimate the total basin snow volume. This method assumes that the snow distribution measured on one day in early April 2009 is

representative of the snow distribution on a given date during a future field campaign. Snow-volume estimates can be combined with snow density measurements to estimate snow-water equivalent (SWE). This method should decrease field time and improve the accuracy of basin estimates of SWE by optimizing snow-depth sampling, which is significantly more variable than snow density. To validate this approach, the relative snow distribution measured during two intensive basin-wide field campaigns is compared to the relative distribution identified by the most accurate binary regression tree. Results show that: 1) elevation, total solar radiation, and local roughness exert the strongest controls on the spatial distribution of snow in the DCEW, 2) tree complexity is directly related to the maximum attainable accuracy, 3) the combination of regions that minimizes sample requirements depends on the desired level of accuracy, and 4) the relative distribution of snow seems to persist in time.

TABLE OF CONTENTS

LIST OF TABLES

LIST OF FIGURES

# CHAPTER 1: INTRODUCTION

Spatially distributed snow depth estimates in mountainous terrain are important for many applications, but challenging to obtain. Reliable hydrologic models require accurate estimates of precipitation and in mountainous regions, and snow is often a large fraction of the annual precipitation in many areas. The spatial distribution of snow influences landscape ecology (Jones, 1999) and the timing and magnitude of stream discharge (Elder et al., 1991). Snowmelt runoff from mountainous regions contributes about 75% of the streamflow in the western United States and is a staple for agricultural, municipal, industrial, and recreational needs (Doesken and Judson, 1996).

Field measurements of snow depth over large areas are not practical. A common method used to spatially distribute point estimates of snow depth is to relate snow distribution, measured in relatively small representative areas, to landscape properties over larger scales. Linear regression has been used in several studies to examine correlations between snow and topography, and model snow depth as a linear function of topographic variables (Elder, 1991; Hosang J, 1991; Bloschl G, 1992). However, success was limited because snow depth is often non-linearly related to topography (Anderton, 2000). Alternatively, binary regression trees, which predict a dependent variable in a hierarchical process by recursively splitting the dataset into increasingly similar groups in a non-linear fashion, can be used to estimate the spatial distribution of snow (Elder, 1998, Balk, 2000), leading to superior estimates when sufficient data is available (Erxleben,

2002). However, these studies were in relatively small basins and used limited samples due to the difficulties of working in mountainous terrain. Larger scale snow distribution data is needed for operational physically-based hydrologic modeling.

Binary regression trees can be spatially restrictive because, unlike multiple regressions, which can predict values outside of the sample space, binary regression can only predict values that were measured. Therefore, they require a large number of samples from the entire region of interest and cannot be extrapolated to regions containing mean values outside the data used to build the tree. Thus, the data requirements are unattainable at large scales if snow data is collected using field measurements.

Aerial light detection and ranging (LiDAR), which is capable of mapping snow depth at large scales (i.e. >200 $km^2$), combined with binary regression trees, can provide information necessary to improve field sampling strategies and expand the spatial extent of detailed snow surveys. Airborne laser scanning is a remote sensing tool used to measure surface elevations by combining knowledge of the speed of light, the location of the laser head in space, and the time from laser pulse transmission to reception (Deems, 2006). Differencing a snow free LiDAR digital elevation model (DEM) from a snow covered DEM can provide an estimate of snow depth at sub-meter horizontal spatial resolution, with vertical accuracy of ~30 cm, and over spatial extents compatible with basin-scale hydrologic needs, provided vegetation can be accurately filtered. Hopkinson et al. (2004) used aerial LiDAR to map snow depth beneath forest canopies with a mean error of 6 cm. LiDAR data from snow-free conditions can be used to derive topographic parameters known to control snow distribution, such as slope, bare-ground elevation.

vegetation height, solar radiation, curvature, surface roughness, and aspect at sub-meter resolutions. Thus, high resolution topographic data derived from a snow-free LiDAR dataset can be used in binary regression trees to delineate snow covered areas into regions with similar snow distributions.

Identification of land units with similar snow distribution would be advantageous during future field campaigns because mean snow depth and density for each unit can be calculated from relatively few point measurements, collected from easily accessible locations. If the relative distribution of snow is fairly constant in time, then the terminal nodes in the regression tree can be adapted to future dates, provided that a sufficient number of field measurements are obtained to capture each region's mean accurately. Mean SWE for each unit can be estimated from the mean measured depth and density of each unit and summed to determine the total basin SWE.

A number of factors influence the marginal benefit of an additional measurement. Regions with deeper snow and larger extents contribute more to total basin estimates than do regions with shallow snow and small extents. Similarly, some variability exists within each discrete region, and the number of measurements needed to accurately estimate the mean snow depth is directly proportional to its snow-depth variance. Therefore, the most efficient sampling strategy must account for the marginal benefit of an additional depth measurement when defining sample requirements for each region. Virtual snow depth sampling strategies can be tested using high-resolution LiDAR data. Accuracy thresholds can be imposed to determine the number of samples required from each region to achieve each threshold. The sampling strategy that requires the fewest samples to achieve the desired level of accuracy can be implemented during future surveys. This method could

decrease field time and improve the accuracy of basin SWE estimates for watershed analyses.

The objectives of this thesis are to 1) demonstrate the ability of LiDAR to map snow distribution, 2) determine the relative importance of various topographic variables for estimating snow depth using binary regression trees with LiDAR snow data, and 3) use the LiDAR snow depth map to design optimal snow sampling strategies for future field campaigns.

# CHAPTER 2: SITE DESCRIPTION

The Dry Creek Experimental Watershed is located in the semi-arid southwestern region of Idaho, USA, and is approximately 16 km northeast of Boise, ID. The DCEW is 26.9 $km^2$ of mountainous and foothills topography with elevations ranging from 1,000 meters at the outlet of Dry Creek to 2,100 meters at the headwaters. Winters in this region are moderately-cold to cold. Precipitation falls mostly as snow in the highlands and rain in the lowlands. Annual snow survey data show that snow depth is primarily controlled by elevation and aspect. Above 5,000 feet elevation, snow usually begins accumulating in November and persists through May on high elevation, north-facing slopes. Snow depth averages approximately 55 cm and rarely exceeds two meters. Vegetation along the Boise Front varies with elevation, geology, microclimate, soil type, and topography. At lower elevations, grass and shrubs dominate, with cottonwoods and ponderosa pine lining the fluvial channels. Upper elevations are dominated by ponderosa pine and Douglas-fir with patches of lodge pole pine and aspen. Middle elevations range from grass and shrubs to open forest communities of ponderosa pine and Douglas-fir. Above approximately 4,000 ft., dense Ceanothus stands are common. Multiple sites in the watershed are instrumented for ongoing investigations into geochemistry, groundwater recharge, infiltration, basin precipitation partitioning, soil water distribution, streamflow generation, and runoff at multiple scales. The DCEW was selected because it is home to extensive ongoing hydrologic research and modeling efforts that can benefit from improved estimates of snow distribution (Aishlin and McNamara, 2011).

# CHAPTER 3: METHODS

## 3.1 Airborne LiDAR Surveys

Two airborne LiDAR surveys were performed over the study site by Watershed Sciences Inc: the first just prior to snow accumulation on November 10, 2008, henceforth, called the snow-off data, and the second near the time of maximum snow accumulation on March 18, 2009, henceforth, called the snow-on data. The Leica ALS50 Phase II laser system, with a sensor scan angle of $\pm 15^{o}$ from nadir, was used for both surveys. The pulse rate was calibrated to yield an average native density of $\geq 6$ points/$m^2$ for the snow-off survey and $\geq 4$ points/$m^2$ for the snow-on survey. The watershed was surveyed with an opposing flight line side-lap of $\geq 50\%$ ($\geq 100\%$ overlap) to reduce laser shadowing and increase surface laser painting. For both flights, the system recorded up to four range measurements per pulse, and all discernible laser returns were processed for the output dataset. To accurately solve for laser point position, the aircraft position was measured at a rate of 2 Hz by an onboard differential GPS unit, and the aircraft attitude was measured at 200 Hz as pitch, roll, and yaw by an onboard inertial measurement unit (IMU). The raw data was calibrated by comparing it to differential GPS ground measurements and aligning flight overlap using TerraScan v.8.001 and TerraMatch v.8.001 software. It was delivered as LAS v. 1.1 files. Each point contained a corresponding scan angle, return number, intensity, and x, y, z information.

### 3.2 LiDAR Point Classification and Bare-Ground DEM Generation

Point data were classified as ground or vegetation using a combination of automated and manual procedures. The publicly available Boise Center Aerospace Laboratory (BCAL) LiDAR tools were used to initially classify the points as ground or vegetation and to derive a preliminary bare ground digital elevation model. These tools are a publicly available ENVI programs (Environment for Visualizing Images), ITT Visual Information Solution, Boulder, CO, USA; (http://bcal.geology.isu.edu/Envitools.shtml; Streuker and Glenn, 2006). The height filtering algorithm embedded in the BCAL LiDAR tools uses an iterative windowed spatial filtering technique to classify points as a function of their relative elevations and the user-defined canopy spacing parameter. A canopy spacing parameter defines the length and width of the moving window used to locate ground points to correspond to the linear distance between ground points in dense vegetation. The tool initially locates the lowest return within the area of interest, equal to the size of the canopy spacing window, and classifies it as ground. All other points are classified as vegetation. It repeats the process for the 8 neighboring cells of equal size. It then fits a surface to the ground points of all 9 cells and reclassifies all points that lie under the initial surface as ground. This process repeats until no more points exist under the surface or for a maximum of 15 iterations.

The BCAL height-filtering algorithm accurately classifies bare ground points in the gently rolling grass and sagebrush dominated lower portion of the watershed. At small canopy spacings, the tool also accurately classifies topographic ridge and peak points as ground, but misclassifies a large number of vegetation points as ground, leading

to excessive commission errors. When the window size is small and the canopy is thick, the tool is unable to find true ground points, but still classifies the lowest elevation points as ground. DEMs created from such a dataset have well defined topography and good ground point density, but numerous artificial elevation spikes caused by misclassified vegetation points that float several meters above the true ground surface (Figures 1a - c).

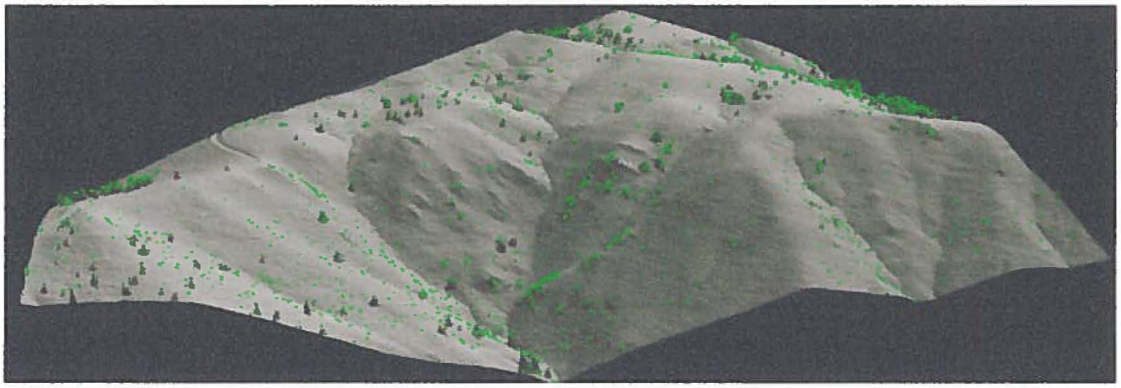

**Figure 1a: Artificial vegetation mounds exist in forested locations when the BCAL LiDAR tools classify ground points using 2.5 meter canopy spacing. Green dots are misclassified ground points.**

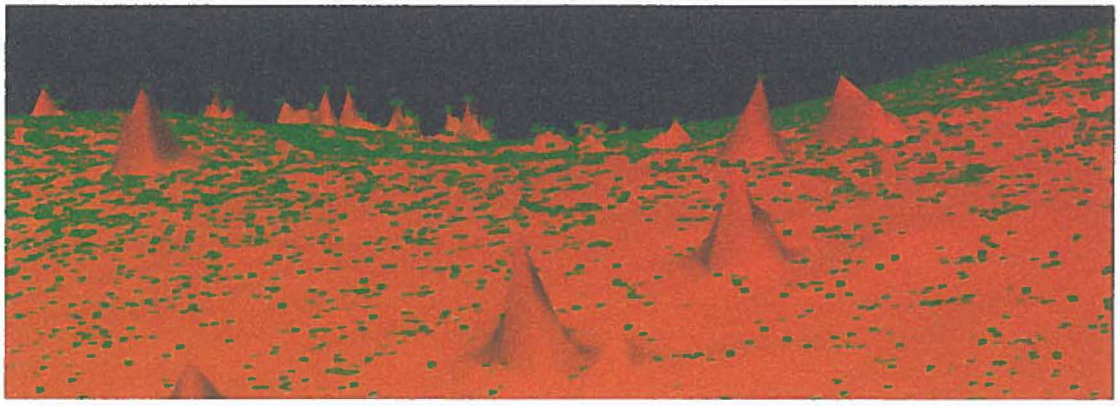

**Figure 1b: Close-up of the artificial vegetation mounds and misclassified points caused by the 2.5 meter canopy spacing. Orange is the bare ground surface created using only the BCAL classified ground points. Green dots are the misclassified ground points that caused the artificial vegetation mounds.**

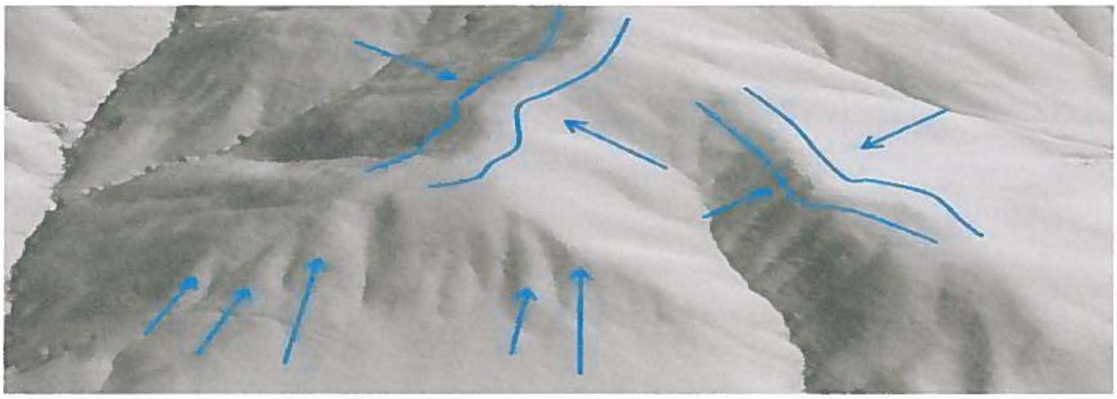

**Figure 1c: Accurate representation of topographic features using 2.5 meter canopy spacing to classify points in areas with rapid slope transitions.**

Conversely, at large canopy spacings, the tool more accurately classifies vegetation points as non-ground because it has more area to search for true ground points, but misclassifies ridges and peaks as non-ground and suffers from poor ground point density. This occurs because the tool locates the lowest elevation returns within the large window sizes, which often span both sides of ridges. Therefore, the initial ground points are those that are furthest down slope on both sides of the ridge, so the surfaces that are fit to the initial points are always below the elevation of the ridge points. The resulting DEMs are mostly free of artificial elevation spikes, but have flat ridges and peaks and fail to capture subtle changes in topography (Figures 2a and 2b).

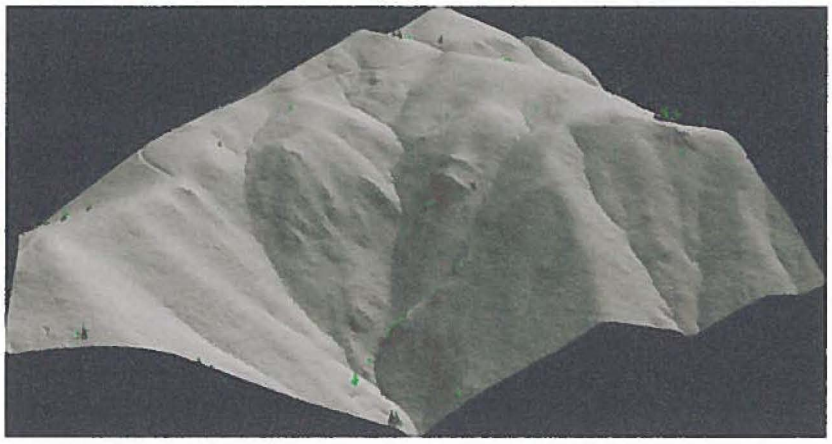

**Figure 2a: The dataset from the 7 meter canopy spacing contained significantly less commission errors than the 2.5 meter spacing. Green dots are misclassified ground points (decided by visual inspection).**

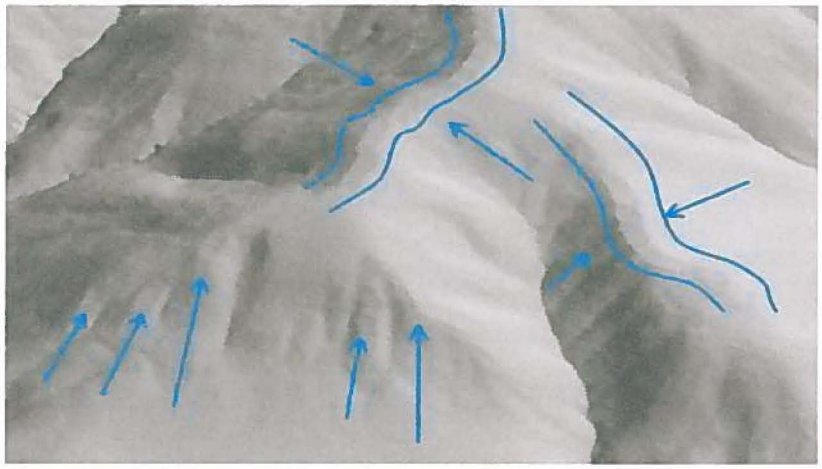

**Figure 2b: 7 meter canopy spacing caused ground points on ridges to be classified as vegetation, resulting in flat ridges, which led to unrealistic snow depths.**

To improve ground point classification accuracy, manual editing tools and automated routines embedded in Quick Terrain Modeler v7.1.1 (QTmodeler) that classify LiDAR points were used in combination with three different ENVI classified datasets with decreasing canopy spacings. QTmodeler enables a user to classify points by visual inspection and to filter and classify points by above ground level (AGL) and a host of other parameters. Combining the ENVI and QTmodeler toolsets made it possible to

systematically increase the true ground point density, remove misclassified vegetation points, add topographic ridge and peak points, and retain information about subtle topographic changes by reclassifying the points misclassified by the BCAL tools.

Snow-off and snow-on DEMs, with vegetation removed, were created using the following workflow to improve the accuracy of the DEMs, by reducing commission and omission errors in the bare ground dataset (Figures 3a - c).

**Figure 3a: Snow free DEM interpolated from all points.**

**Figure 3b: Snow-free bare ground DEM created from only ground points, defined by BCAL LiDAR tools, using 2.5m canopy spacing. Light color is the bare ground surface. Dark color is the vegetation.**

**Figure 3c: Snow free bare ground DEM created from multi-level filtering, Steps 1-12.**

1) Process point data using BCAL tools and a 7m canopy spacing. This spacing was large enough to remove the majority of vegetation, but suffered from significant ground point omission errors, especially on ridges.
2) Specify gridding extent and origin. Interpolate the ground points using natural neighbors and cell sizes that are equal to the average point spacing.
3) Use the artificial vegetation mounds in the DEM from Step 2 to locate the misclassified ground points from Step 1 and manually reclassify them. This removed commission errors. Mounds were considered to be artificial if the slope of the interpolated surface was greater than 80 degrees at the location of the point. If they formed a rounded shape with no clear apex, they remained in the ground class.
4) Interpolate the remaining points from Step 3 using same method, origin, and spacing as Step 2.
5) Process the raw point data using a 4 meter canopy spacing. This canopy spacing significantly reduced omission error, but increased commission error (with respect to the ground point class).
6) Use the bare ground estimate created in Step 4 to calculate an above ground height for each ground point classified in Step 5.
7) Remove all ground points from Step 6 that are greater than 1 meter above the ground DEM created with the 7m canopy spacing. This reduced commission errors because they mostly occurred in canopies of dense conifer stands, with

AGL values greater than 1 meter. The 1 meter threshold also minimized omission error because most of the misclassified ground points were on ridges and areas with subtle topographic changes and were almost always less than 1 meter above the DEM created in Step 4.

8) Interpolate the remaining points from Step 7 using same method as Step 2.
9) Use the DEM from Step 8 to locate the misclassified points causing artificial vegetation mounds and manually reclassify them. Mounds were considered to be artificial when the interpolated surface was greater than 80 degrees at the location of the point. At this step, false ground points were primarily located in the dense ceanothus patches, with returns coming from the large woody stems of the plant.
10) Interpolate the remaining points from Step 9 using same method as Step 2.
11) Process raw point data using a 2.5 meter canopy spacing.
12) Repeat steps 6 – 10 using the processed data from Step 11.

### 3.3 LiDAR Estimates of Snow Depth

Snow depths were initially calculated by differencing the DEMs from the snow-off and snow-on flights, after the DEMs were interpolated to a regular grid with the same spacing and origin. This improved snow depth estimates (relative to unaligned grids), especially in steep terrain, because only points within the same spatial domain were interpolated and differenced. This differs from previous studies (Deems et al., 2006) in which one DEM point cloud was interpolated to the locations of the point cloud in the second flight (only 1 DEM was interpolated).

Six different snow depth maps were created to determine the canopy spacing that produces the most accurate snow-depth estimates, and to evaluate if increasing the

ground point density and DEM resolution improves snow-depth estimates. LiDAR snow depth error statistics were calculated for each map by comparing the LiDAR and measured snow depths.

To determine the optimal canopy spacing, snow depth DEMs were created from 7, 4, and 2.5 meter windows and interpolated using just the BCAL classified ground points, edited for commission errors using the appropriate components of Steps 1-12 above. These spacings were chosen because they correspond to the range of canopy densities observed in the watershed.

To determine the effect of ground point density, all points within 10 cm of the cleaned bare ground estimate were re-classified as ground for all three canopy spacings. The effect of adding ground points was important to examine because the ENVI filter classifies only the lowest points in a window as ground, removing information about subtle topographic changes (Figures 4a).

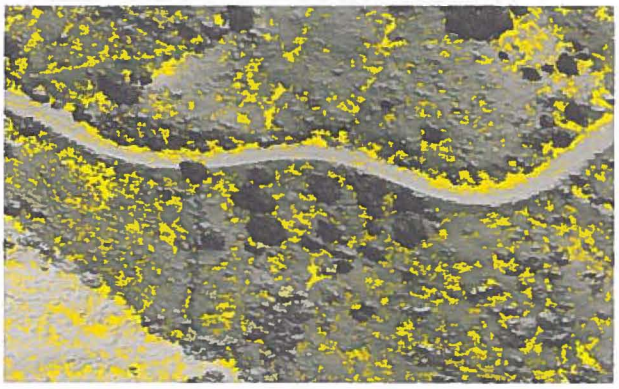

**Figure 4a: Yellow points are classified ground points using BCAL tools and a 4 m canopy spacing, cleaned using Steps 1 – 10. Background DEM is the interpolated surface of all points.**

**Figure 4b: Green points are ENVI classified ground points using BCAL tools and a 4 m canopy spacing, cleaned using Steps 1 – 10, with the addition of all points within 10 cm of the interpolated surface. Background DEM is the interpolated surface of all points.**

Therefore, reclassifying all points within 10 cm AGL significantly increased ground point density, revealing small-scale topography, important to snow depth estimates, with only minor increases in commission error. The 10 cm threshold was chosen because it captured the majority of road points, without including any obvious vegetation points in surrounding areas (Figure 4b) and should therefore decrease omission errors. Each of the six datasets was interpolated to cell sizes equal to the average ground point spacing.

An analysis of the snow-free region from all 6 resulting DEMs of difference (DOD) revealed a vast number of non-zero values (>95%). To identify any systematic bias in the snow-depth estimates, 50,000 random points were selected from a paved road within the study area, which was snow free during both flights. At each point, error (any non-zero value), slope, aspect, elevation, easting, northing, curvature, and elevation were extracted. Error was plotted against each topographic variable. Easting, northing, slope, and elevation had the strongest correlations with error (Figures 5a-d).

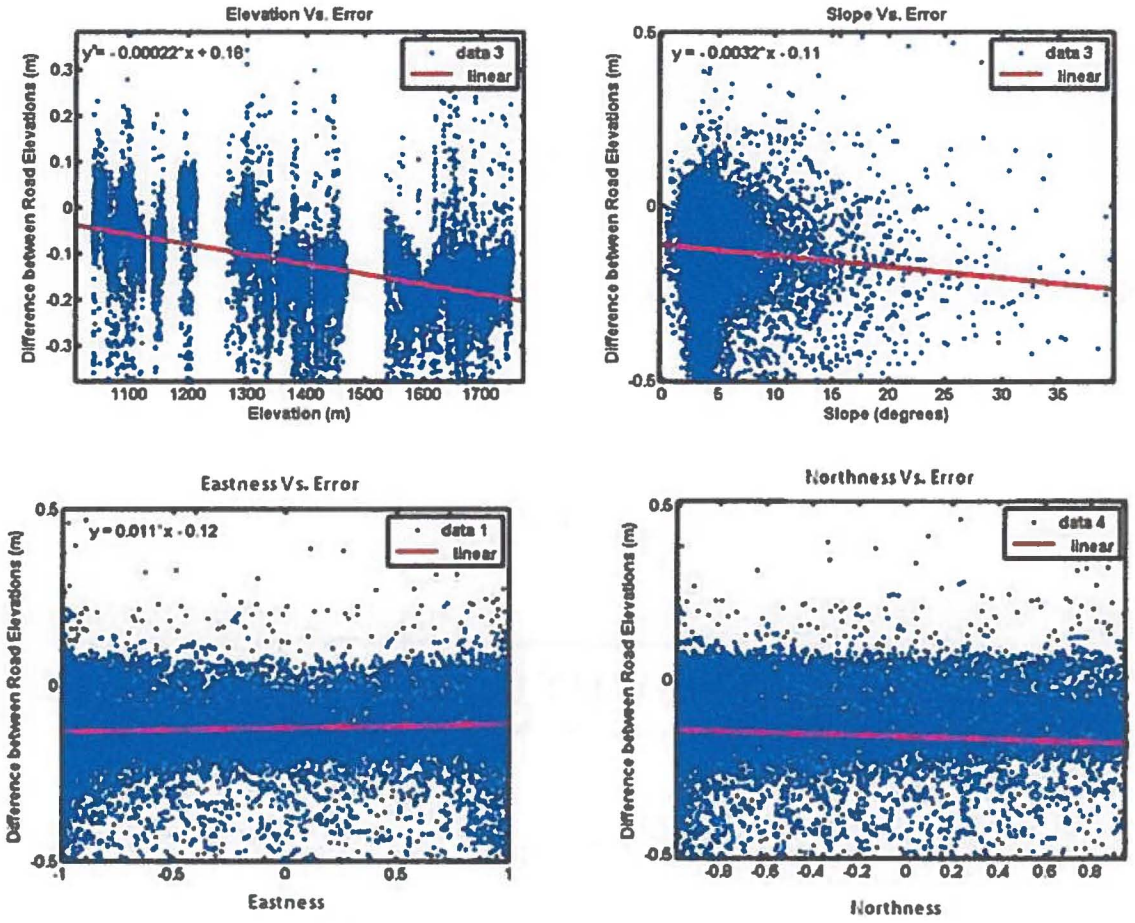


**Figure 5a-d: Values from the differenced LiDAR DEMs, extracted from Bogus Basin road, plotted against: 5a: elevation 5b: slope 5c: eastness 5d: northness**

Robust multiple regression, an iterative process used to weight points as a function of their distance from the predicted best fit line, was then used to predict error as a function of the four independent variables in a least squares sense. This improved error prediction by minimizing the influence of outliers caused by misclassified points or differences in LiDAR return locations within each cell, between flights, in extremely rough terrain. Since the range and magnitude of errors varied slightly between the six snow-depth maps, a unique offset map was calculated for each one. The offset maps were used to estimate the expected error for each cell of the corresponding snow depth

maps. The resulting offset equation for the snow depth map used in the final analysis had an RMSE of 0.095 (Equation 1) and was used to construct a grid of offset values for the 4mR98cm snow depth map (Figure 6). The offsets ranged from -0.58 to 0.07 meters.

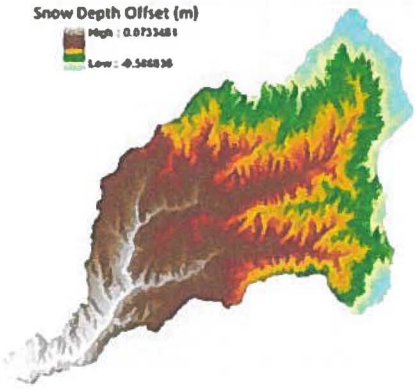


Offset = Slope * – 0.00030927 + Northness * 0.0357 - Eastness* 0.0675 - Elevation * 0.00057218 + 0.5946

**Figure 6: Snow Depth offset for 4mR98cm snow depth map.**

The final snow depth maps were derived by subtracting the offsets from the original maps. The snow depth estimates from all six corrected maps were then compared to the measured snow depths to calculate bias and to determine the single best map for use in the binary regression tree (Table 1).

**Table 1: Statistics for LiDAR snow depth errors for all models, using 82 measurements and 5 transects. Note: first number is canopy spacing parameter. Second number is the raster resolution. For example, 7mR1m = 7 meter canopy spacing and a 1 meter cell size. Bad Pixel = snow depth < -0.30 (2x absolute vertical accuracy of raw point cloud) or snow depth > 3.0m (1.9 meters greater than maximum observed snow depth).**

| | 7mR1cm | 7mR72cm | 4mR98cm | 4mR67cm | 2.5mR91cm | 2.5mR63cm |
|---|---|---|---|---|---|---|
| **Mean** | -0.054 | -0.038 | -0.019 | -0.063 | -0.086 | -0.074 |
| **Mode** | -0.117 | -0.106 | 0.053 | -0.007 | -0.107 | 0.013 |
| **Median** | -0.086 | -0.063 | 0.002 | -0.052 | -0.073 | -0.056 |
| **Variance** | 0.053 | 0.050 | 0.047 | 0.051 | 0.061 | 0.062 |
| **Std Dev** | 0.231 | 0.223 | 0.217 | 0.226 | 0.246 | 0.249 |
| **Inter Quartile Range** | 0.291 | 0.273 | 0.242 | 0.2676 | 0.2968 | 0.2645 |

| | | | | | | |
|---|---|---|---|---|---|---|
| **Skewness** | 0.478 | 0.545 | 0.371 | 0.536 | 0.493 | 0.412 |
| **Kurtosis** | 3.760 | 3.923 | 4.829 | 4.373 | 4.826 | 4.040 |
| **Percent Bad Pixels** | 2.976 | 2.946 | 0.601 | 0.585 | 0.492 | 0.322 |

The error offset from the regression equation was chosen over a standard offset, equal to the bias, because although they both decreased the bias, the regression offset decreased the range and variance of snow-depth errors.

### 3.4 LiDAR Estimates of Topography

Topographic parameters were calculated from the snow-off dataset at a 1 meter resolution using automated procedures in ENVI and ArcGIS and the point data that corresponded with the spatial extent of each 1 $m^2$ raster cell. Slope, aspect, total solar radiation, direct solar radiation, diffuse solar radiation, duration of direct solar radiation, plan curvature, cross-sectional curvature, and profile curvature were calculated in ArcGIS.

The curvature tool embedded in ArcMap's Spatial Analyst toolbox estimates curvature as the second derivative of slope for a surface fit through a point of interest and its 8 neighboring cells. Curvature values were calculated from a 2 $m^2$ DEM because at finer resolutions, the linear distance between neighboring cells was too small to capture the shape of ridges, depressions, and channels and resulted in a chaotic distribution of curvature values with no discernible relationship to topographic features. The coarser resolution produced a more continuous DEM with pronounced ridges and depressions.

SOLARFLUX, an ESRI tool used to calculate solar insolation for complex surfaces based on solar angle, surface orientation, slope, shadowing due to topographic

features, and atmospheric attenuation, was used to calculate all four solar radiation parameters, assuming clear sky conditions. For fine resolution DEMs, SOLARFLUX requires significant processing time (3 days to process the 27 $km^2$ watershed using 1 $m^2$ cells for a 24 hour solar radiation estimate), making cumulative seasonal radiation estimates impractical. Initially, solar radiation values were calculated for the 18$^{th}$ of every month, starting in November and ending in March. However, when the summed values were used in the regression trees, total incoming solar radiation was only minimally important. As a result, it was assumed that the relative distribution of solar radiation at the onset of the melt season is more important for predicting snow distribution on March 18$^{th}$ than its distribution during the accumulation period. Therefore, solar radiation values were averaged for March 1$^{st}$, 9$^{th}$, and 18$^{th}$ and used as an index to solar radiation inputs at the onset of the melt season. This improved the predictive ability of the solar radiation variables. The shade produced by canopy structure was not captured in the SOLARFLUX calculation. However, mean vegetation height and local roughness were used as potential analogs to canopy effects.

The BCAL LiDAR tools were used to calculate the mean vegetation height, absolute roughness, local roughness, and vegetation roughness. Local roughness is the standard deviation of elevation for each point, de-trended for slope. Absolute roughness is the standard deviation of elevation. Vegetation height is the mean above ground height for all non-ground classified points. Vegetation roughness is the standard deviation of above ground height for all non-ground points.

Molotch et al., 2003, found that the addition of *northness* (=cos (aspect) * sin(slope)) improved regression tree performance in the Tokopah Basin, NV. Therefore,

northness was calculated from 1 meter resolution slope and aspect maps and added as a predictor variable.

### 3.5 Measured Snow Depths

On the day of the snow-on flight, 82 georeferenced snow depths were collected in 5 different transects using a depth probe and a Trimble 5700 differential GPS unit (Figure 7).

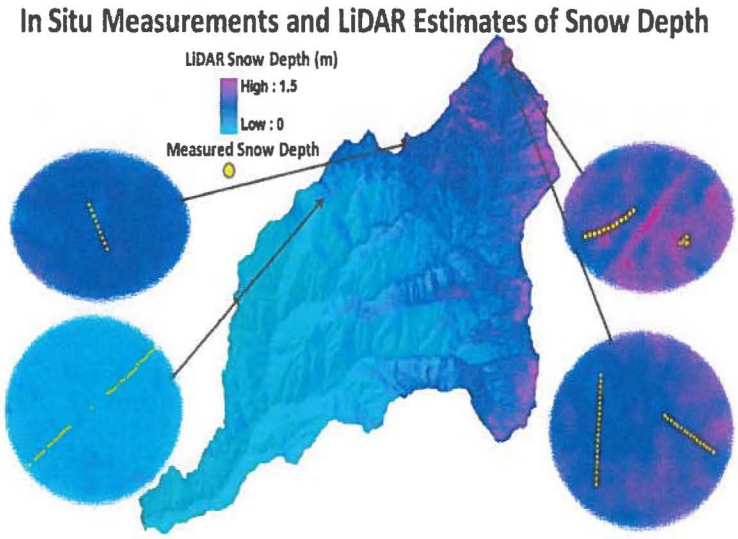


**Figure 7: Locations of measured snow depths shown on top of the LiDAR snow depth map that used for the final analysis.**

The locations were selected to capture the range of snow depths expected in the watershed based on previous basin wide snow surveys. Snow-water equivalent measurements were made at the endpoints of each transect using a Federal snow sampler.

### 3.6 SWE Map

Snow water equivalent (SWE) was calculated for every pixel as follows:

$$SWE_p = d_p * (\rho_s \div \rho_w) \quad (2)$$

where $d_p$ (m) is the LiDAR snow-depth estimate for the pixel of interest, $\rho_s$ (kg $m^{-3}$) is the mean snow density measured on 3/18/09, $\rho_w$ is the mean density of water (kg $m^{-3}$). Mean snow density was used in place of modeled estimates because the sample size was too limited for spatially distributed estimates and because previous studies have shown that snow density is significantly less variable than snow depth (Figures 8a-b).

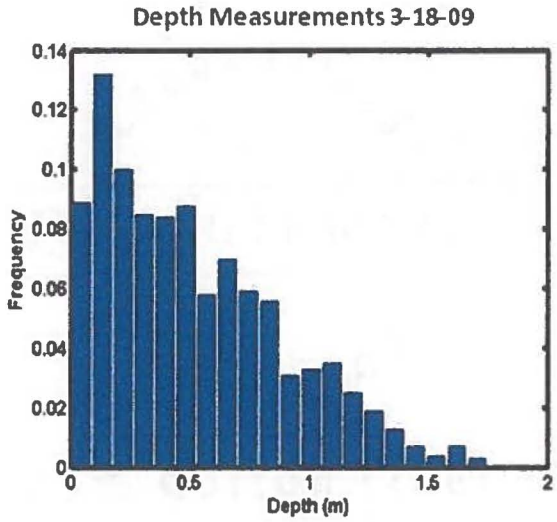


**Figure 8a: Distribution of depth measurements from basin-wide survey, 3-18-2009.**

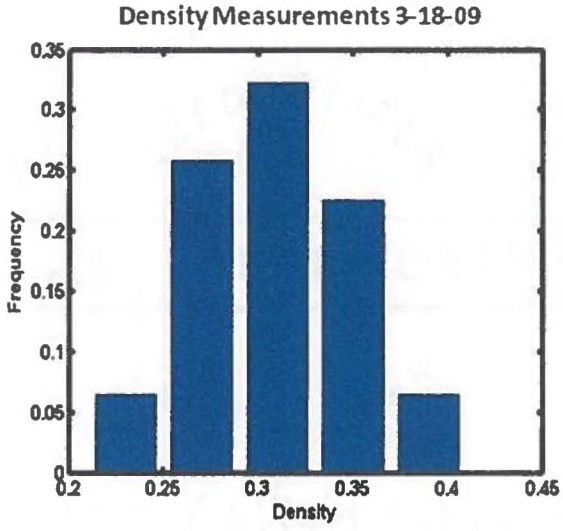


**Figure 8b: Distribution of density measurements from basin-wide survey, 3-18-2009.**

### 3.7 Binary Regression Trees

Binary recursive partitioning was used to bin a random sample of 5 million snow depths into increasingly homogeneous subsets as a function of the 16 corresponding topographic variables. All independent variables were examined at each decision split, and the single variable that minimized deviance in the resulting subsets was selected. Nodes were split when it minimized the total class variance and the children contained a predefined minimum number of observations.

The optimal tree size depends on the purpose of the regression and there can be a tradeoff between accuracy and tree size. The optimal tree suggested here for operational snow sampling campaigns discretizes the watershed into regions that require the least samples to achieve accuracy thresholds for total basin snow volume. To find the optimal tree size, minimum leaf requirements of 1-12% of all LiDAR observations were imposed using the MATLAB code discussed below. Henceforth, individual regression trees are

named by the fraction of total snow depths that were used as minimum leaf requirements during their construction.

All regression trees were initially grown to over-fit the data (Chambers and Hastie, 1993). Ten-fold cross-validation was then used to calculate the cost (MSE) associated with each node, as well as, the total cost associated with all trees sizes. The final trees were constructed by pruning decision splits so that the resultant trees' MSE was within one standard error of the minimum cost sub tree (Breimen et. al, 1984).

### 3.8 Estimation of Appropriate Sample Sizes

An algorithm was created in MATLAB to perform virtual snow sampling campaigns on the LiDAR data, to identify the optimal snow survey strategies. The optimal survey for a set of discrete regions allocates samples efficiently and minimizes the sample size needed to meet accuracy thresholds for the total basin snow volume estimates. One approach is to locate easily accessible subsections of each discrete region, identified by the regression trees, collect enough random samples to obtain an acceptable estimate of the true mean, and multiply the estimated mean snow depth by each region's area. Then, each region's snow volume estimate can be summed to estimate the basin's total snow volume.

The code accounts for the variability of marginal benefits from an additional sample and identifies the optimal sampling strategy by identifying the combination of discrete regions and corresponding sample sizes that require the fewest measurements to meet total basin snow volume accuracy thresholds. It uses 5 million randomly selected snow depths and sixteen topographic parameters to create a regression tree and then utilizes the pruned and cross-validated tree to assign each pixel to a discrete region, as a

function of the corresponding topographic parameters. The 5 million points (~26% of the positive snow depths) are subset for this portion of the code because, with the addition of topographic variables, the dataset overwhelms computational resources.

For each discrete region, a Monte-Carlo simulation is performed to randomly locate a single point in each region. It uses the random sample from the 5 million extracted points to locate the original cell in the gridded dataset, and uses the grid to draw 1+ n (n=1:121) random samples from all points within the region that are also within 5 meters of the initial point, and calculates the mean absolute deviation (MAD) of the difference between the mean of all n samples and the true mean. The 5 meter threshold was chosen because it coincides with an area that is easy to sample in the field. The MAD of snow volume was used because it captures the positive and negative bias. This simulation repeats 5,000 times for each sample size and then calculates the mean of the mean absolute deviations from the 5,000 mean snow depth estimates of each sample size.

To calculate the mean absolute snow volume error for each sample size, the mean absolute deviation of each sample size is multiplied by each region's corresponding area. Because the 5 million points were randomly sampled from the entire snow covered area, it was possible to estimate each region's area by multiplying the fraction of samples located in each region by the total snow covered area. The marginal benefit of an additional sample is defined as the reduction in the MAD of snow volume per additional sample. It is estimated by differencing the mean absolute snow volume error of sample size n and n+1 for n=1:121. However, in some regions, random effects were strong enough that an increase of only 1 measurement sometimes led to slight local increases in bias (Figure 9a). Therefore, points would no longer be assigned to these regions because

it seemed to increase the error, even though the overall trend was a decrease in bias with increasing sample size. To minimize the influence of random effects, the MAD of snow volume estimates is modeled as a function of sample size with a non-parametric smoothing function using a bisquare kernel of three samples (Figure 9b).

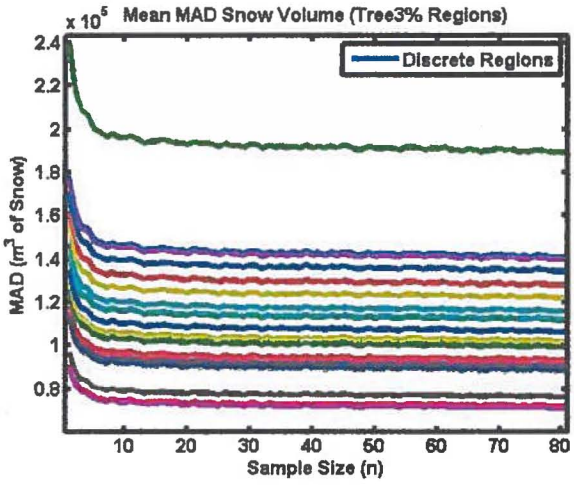


**Figure 9a: Mean absolute deviation of snow volume plotted as a function of sample size for each discrete region.**

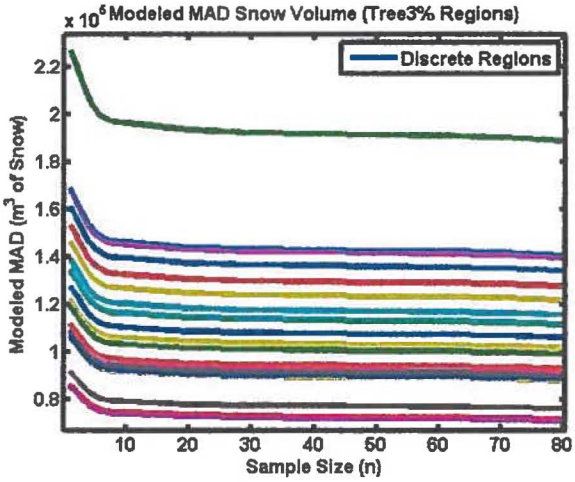


**Figure 9b: Modeled estimates of the mean absolute snow volume error, plotted as a function of sample size for each discrete region.**

To estimate the marginal benefit of an additional point, the modeled estimates for the MAD of snow volume are evaluated and differenced at sample size n and n + 1. The region with the maximum marginal benefit is assigned an extra point. The code then uses the sample sizes from each region to find the 5,000 corresponding snow volume estimates that were calculated in the previous Monte-Carlo simulations. For 1,500 loops, the mean snow volume estimates that correspond to each region's assigned sample size are randomly sampled and summed to estimate the basin's total snow volume at the current loop's sample size. For each of the 1,500 estimates of total basin snow volume, the fraction of bias is calculated by dividing the random sample's estimate of the total basin snow volume by the true basin snow volume and subtracting one. If less than 95% of the total basin snow volume estimates are within the current loop's accuracy threshold (± 8 % : ± 50% of the true snow volume), the marginal benefit for the region that received an extra point is recalculated and the process repeats until 95% of the snow volume estimates are within the accuracy threshold for total basin snow volume.

Once the thresholds are met, the samples from each region are summed and the code repeats with new minimum leaf requirements of 1%: 12% of the total dataset (henceforth, trees are identified by their minimum leaf requirements). The total sample requirements from each regression tree and accuracy threshold are compared. The combination of discrete regions and sample sizes that minimize total sample requirements for each threshold is suggested for use during future field campaigns.

### 3.9 Validation of Discrete Regions

Basin-wide field surveys were performed on March 2, 2011 and April 8, 2011. They were designed to determine the variability in the relative distribution of snow at

near peak accumulation. Tree 2%'s thirty-four discrete regions were sampled. This tree was chosen because it contained the most regions that a six person field crew could sample in a day.

Within each region, easily accessible locations were selected to sample (Figure 10a and b).

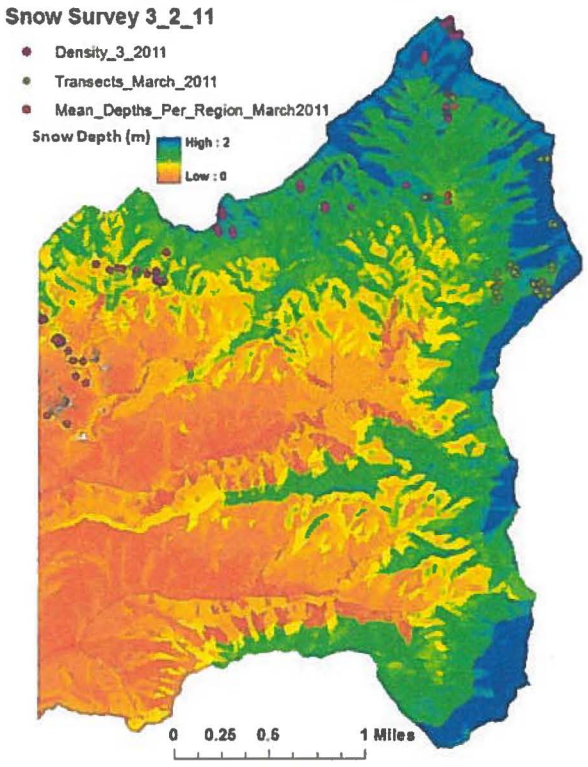


**Figure 10a: Sample locations for the 2 basin-wide snow survey (3/2/11).**

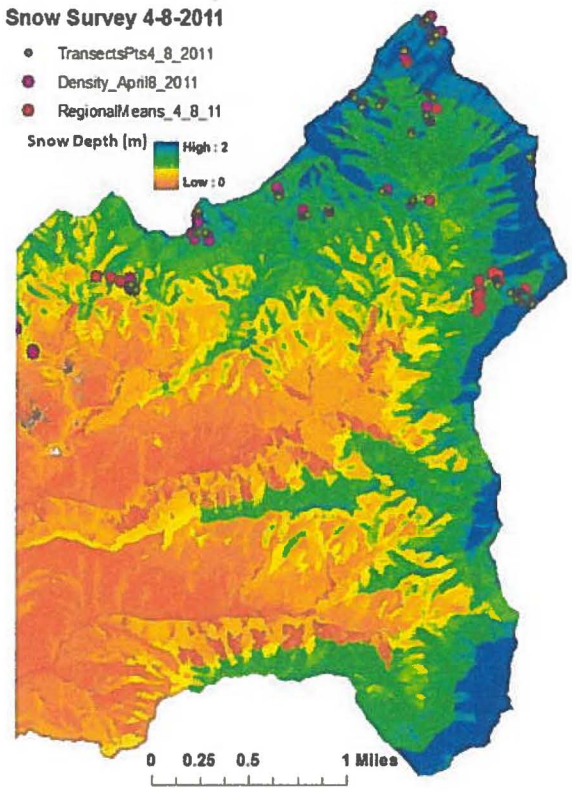


**Figure 10b: Sample locations for the 2 basin-wide snow survey (4/8/11).**

At each location, sixty random depth measurements were collected within a 5 meter radius. Twenty-one additional fifty meter transects were surveyed for another study. All points were georeferenced and the topographic parameters that were used to make the regression tree were extracted at the location of each sample. The values of the topographic variables were evaluated using Tree1% to assign each point to a discrete region. These points were combined with the randomly sampled depths to estimate the mean snow depth for each discrete region.

To compare the relative snow distribution between the LiDAR survey and the two field surveys, the mean depth for each region and date was normalized by the depth of the region with the maximum mean snow depth on the corresponding date.

### 3.10 Variable Importance

To improve our understanding of the topographic controls on snow depth, the regression tree was used to estimate the predictive ability of each variable as follows:

$$I(j) = E\left(\sigma^2_{\text{parent}(j,k)} * \frac{\text{nparent}(j,k)}{N} - \left(\sigma^2_{\text{child1}(j,k)} * \frac{\text{nchild1}(j,k)}{N} + \sigma^2_{\text{child2}(j,k)} * \frac{\text{nchild2}}{N}\right)\right) \quad (3)$$

where j = the $j_{th}$ independent variable and k = the $k_{th}$ instance of the $j_{th}$ variable in the regression tree.

Tree1%'s pruned tree was used for the variance reduction calculations because it was the least constrained and most accurate.

### 3.11 Accuracy Assessment

To assess the performance of the regression trees, a validation dataset of 5 million random points was fit to each tree as a function of the topographic parameters, using MATLAB's eval function. Prediction error was defined as the difference between the LiDAR depth estimate and the regression trees' modeled estimates and was calculated as follows:

$$\textbf{Error}_{\text{pixel}} = \textbf{Snow Depth}_{\text{predicted}} - \textbf{Snow Depth}_{\text{LiDAR}} \quad (4)$$

Statistics were calculated for the distribution of errors for modeled depth estimates and tabulated in Table 2.

**Table 2: Error statistics for the regression tree snow depth models**

| | Tree1% | Tree2% | Tree3% | Tree4% | Tree5% | Tree6% | Tree7% | Tree8% | Tree9 -10% | Tree1 1-12% |
|---|---|---|---|---|---|---|---|---|---|---|
| # Leaves | 69 | 34 | 22 | 18 | 14 | 12 | 10 | 9 | 7 | 6 |
| $R^2$ | 0.680 | 0.654 | 0.639 | 0.612 | 0.610 | 0.593 | 0.589 | 0.580 | 0.557 | 0.525 |

| | | | | | | | | | | |
|---|---|---|---|---|---|---|---|---|---|---|
| **μ error (m)** | 0.0081 | 0.0083 | 0.0084 | 0.0086 | 0.0086 | 0.0088 | 0.0088 | 0.0089 | 0.0088 | 0.0090 |
| **Median error** | 0.023 | 0.026 | 0.028 | 0.031 | 0.032 | 0.033 | 0.033 | 0.035 | 0.035 | 0.042 |
| **σ2 of Error** | 0.049 | 0.053 | 0.055 | 0.059 | 0.059 | 0.063 | 0.063 | 0.064 | 0.067 | 0.068 |
| **σ of error** | 0.221 | 0.229 | 0.234 | 0.243 | 0.244 | 0.250 | 0.250 | 0.253 | 0.260 | 0.261 |
| **MSE** | 0.049 | 0.053 | 0.055 | 0.059 | 0.059 | 0.063 | 0.063 | 0.064 | 0.068 | 0.068 |
| **IQ Range** | 0.243 | 0.253 | 0.262 | 0.274 | 0.274 | 0.282 | 0.282 | 0.290 | 0.298 | 0.300 |

# CHAPTER 4: RESULTS AND DISCUSSION

## 4.1 LiDAR Snow Depth Map

The LiDAR-derived snow depth map (Figure 9) and SWE map (Figure 11a) agree reasonably well with field-mapped estimates of SWE (Figure 11b).

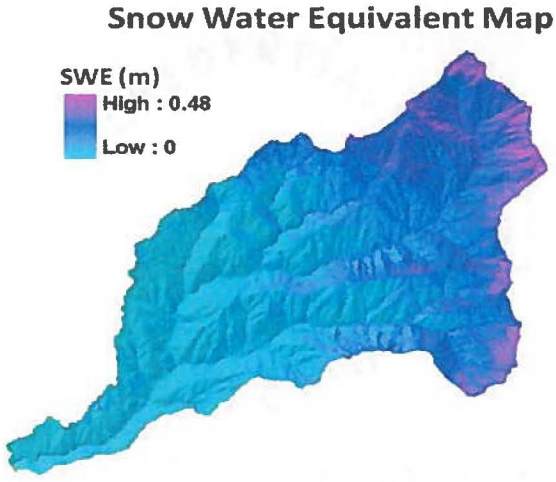


**Figure 11a: LiDAR estimates of SWE, using measured mean density of 0.30.**

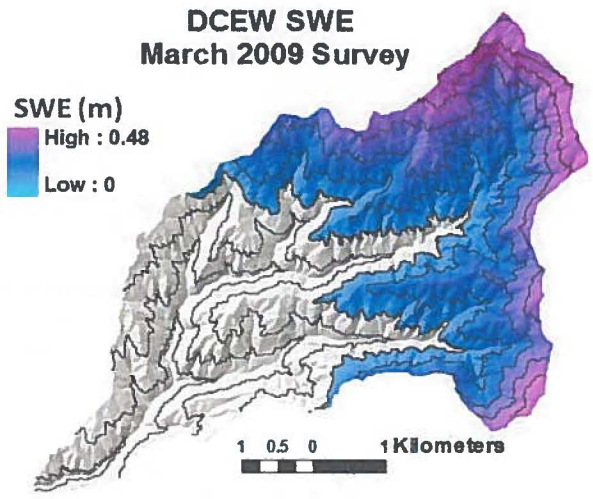


**Figure 11b: Mean measured depths at 1,000 meter elevation bands converted to SWE using mean density of 0.30.**

The surveyed SWE map was constructed by dividing the watershed into elevation bands and averaging the depth and density measurements located within each bin. Consequently, it lacks the detail within elevation zones that are evident in the LiDAR SWE map. Elevation alone is insufficient to discretize the watershed into homogeneous snow units. Total snow and SWE estimates for March 18, 2009 were calculated by summing the cell values in the corresponding maps. LiDAR estimates were 7.81E+06 $m^3$ of snow, 2.34E+06 $m^3$ of SWE, and an average SWE depth of 13 cm, while surveyed estimates were 5.50E+06 $m^3$ of snow, 1.65E+06 $m^3$ of SWE, and an average SWE depth of 11.4 cm.

### 4.2 LiDAR Snow Depth Accuracy Assessment

The multi-level point classification process (Steps 1-12) decreased point classification errors, enabling the creation of maps with both, well-defined topography and few misclassified vegetation points. Decreasing the canopy spacing and increasing

the ground point density and raster resolution decreased the number of bad pixels in all models, but had variable effects on the accuracy of snow depth estimates (Table 1). Bad pixels are defined as snow depths less than -0.3 or greater than 3 meters. Decreasing the cell size decreased the number of unrealistic snow depths because only LiDAR points with close proximity were interpolated and differenced. This was important because in steep terrain, like the DCEW, elevation varies significantly with small horizontal differences in position. Therefore, smaller cells increased the horizontal resolution and improved the vertical accuracy, resulting in fewer pixels with extreme values. Similarly, as ground point density increased and cell size decreased, the accuracy of snow depth estimates improved for the maps derived from the 2.5 and 7 meter canopy spacings, but diminished as points were added to the 4mR98cm map to create the 4mR67cm map. An investigation into this discrepancy is beyond the scope of this paper.

Decreasing the canopy spacing increased ground point classification accuracy in rough terrain and at slope transitions such as road edges and ridges, improving topographic representations and the accuracy of the related snow depths. As the canopy spacing decreased, the number of bad pixels correspondingly decreased. Therefore, maps created from the 4 and 7 meter canopy spacings contained more pixels with unrealistically large positive and negative values at slope breaks because true ground points were sparse and erratic. Future studies may benefit from a point classification algorithm, capable of automatic local canopy spacing parameter adjustments, which responds to differences in vegetation density and terrain features.

Snow depths from the 4mR98cm map lined up the best with physical measurements. However, the 4mR98cm map contained 86% more bad pixels at slope

breaks, which are important to snow distribution, than the 2.5mR63cm DEM. To get the best possible snow depth map, snow depths from ridges were extracted from the 2.5mR63cm map (Steps 1-12), resampled to 98cm, and mosaiced with the non-ridge portion of the 4mR98cm DEM.

Ridges were extracted by gridding the bare earth data points to 10 meter cells to provide a buffer for the ridge features, calculating the flow direction, and then calculating the flow accumulation for each cell using ArcGIS 9.2. Cells with flow accumulation values of zero (Figure 12) were considered ridges and used as a mask to extract snow depths from the 2.5mR98cm snow depth map.

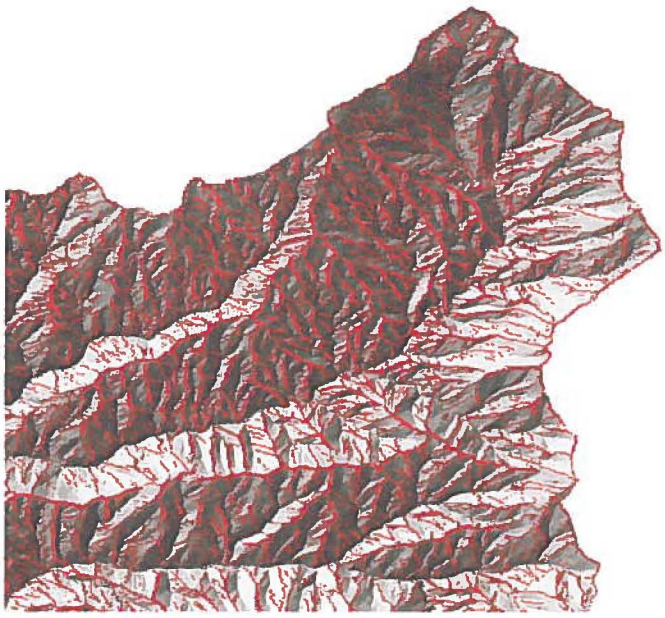

**Figure 12: Ridges classified by flow accumulation values. Red = flow accumulation = 0 = Ridges. The snow depths from the 2.5mR98cm DEM were extracted from cells with no flow accumulation and merged with snow depths from the 4mR98cm map's non-ridge locations to maximize the accuracy of snow depth estimates.**

The appropriate sections of the two maps were mosiaced and the resulting map (Figure 9) was used in the subsequent analysis because it contained both, well-defined peaks and ridges from the 2.5mR98cm map, and the more accurate snow-depth estimates in non-ridge areas from the 4mR98cm map. Error statistics for the combined DEM are the same as the 4mR98cm DEM because no snow depths were measured at the ridge locations.

Snow depth offsets from the robust regression equation improved the accuracy and precision of the snow-depth estimates (Figure 13a and b).

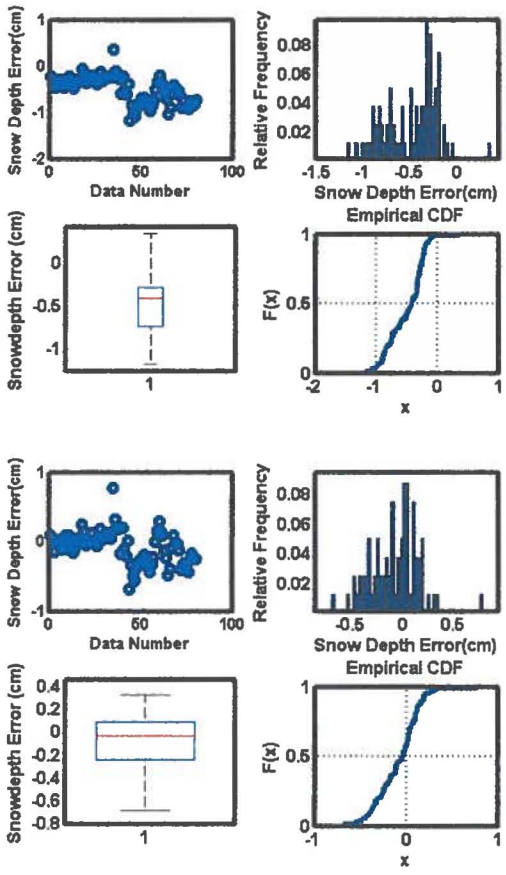


**Figures 13a and b: LiDAR errors (LiDAR depths – measured depths). 13a) Lidar snow depth errors, pre offset, for the mixed 4mR98cm and 2.5mR98cm maps. 13b)**

**Lidar snow depth errors, post offset, for the mixed 4mR98cm and 2.5mR98cm maps.**

A comparison of the corrected LiDAR snow-depth estimates from the combined snow depth map and measurements from the same locations shows that the LiDAR estimates are relatively unbiased, with a median error of 1 cm, 50% of the data within 20 cm of the true value, and 95% of the data between + 30 cm and -70 cm. This indicates that 1) LiDAR may only be viable for point estimates in deep snow because, depending on the application, the magnitude of error may be considered negligible, compared to the snow depths, and 2) LiDAR can be used in shallow snowpacks for accurate areal estimates because the errors are relatively unbiased, but not for point estimates because the magnitude of the errors are on par with snow depths.

The large negative snow depth errors have two likely sources. Over 50% of the measured snow depths were from open locations, with good GPS signals, at higher elevations, which is home to Ceanothus (Figure 14a and b).

**Figure 14a and b: Photos of Ceanothus patch during snow free conditions.**

During the snow-off flight, it is likely that few LiDAR pulses were able to penetrate the thick Ceanothus patches and that some returns from the woody stems were misclassified as ground. As a result, the bare ground surface elevation was probably over-estimated in these locations. However, during the snow-on LiDAR flight, the weight of the overlying snow compressed the Ceanothus and forced it to flatten out on the ground (Figures 15c and d). Therefore, when the two DEMs were differenced, snow depths were likely under-estimated in locations with dense Ceanothus.

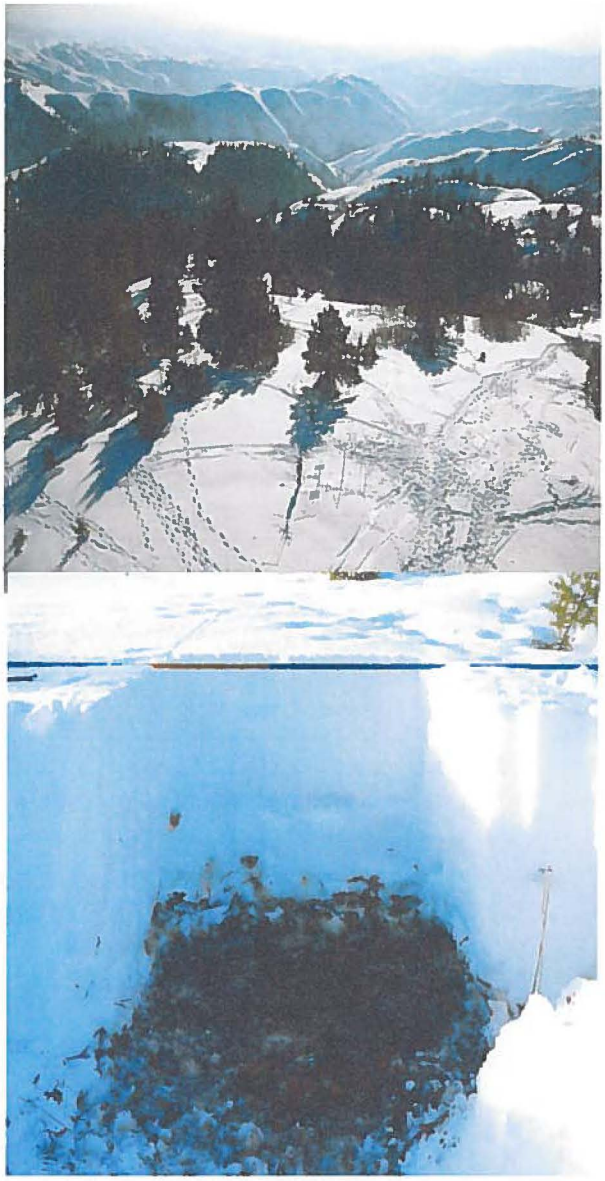

**Figures 15a & b: 15a: Photo of same Ceanothus patch, but covered by snow. 15b: Ceanothus is completely flattened under the weight of snow.**

### 4.3 Regression Tree Performance

The most common metric for regression tree performance comparisons is the coefficient of determination (Molotch et al., 2003, Erxleben et al. 2002, Winstral et al., 2002, Balk and Elder, 2000, Elder et al., 1995). However, comparisons to previous

studies are tenuous because different tree sizes are used for different applications, and $R^2$ values typically increase with the number of terminal nodes (Figure 16).

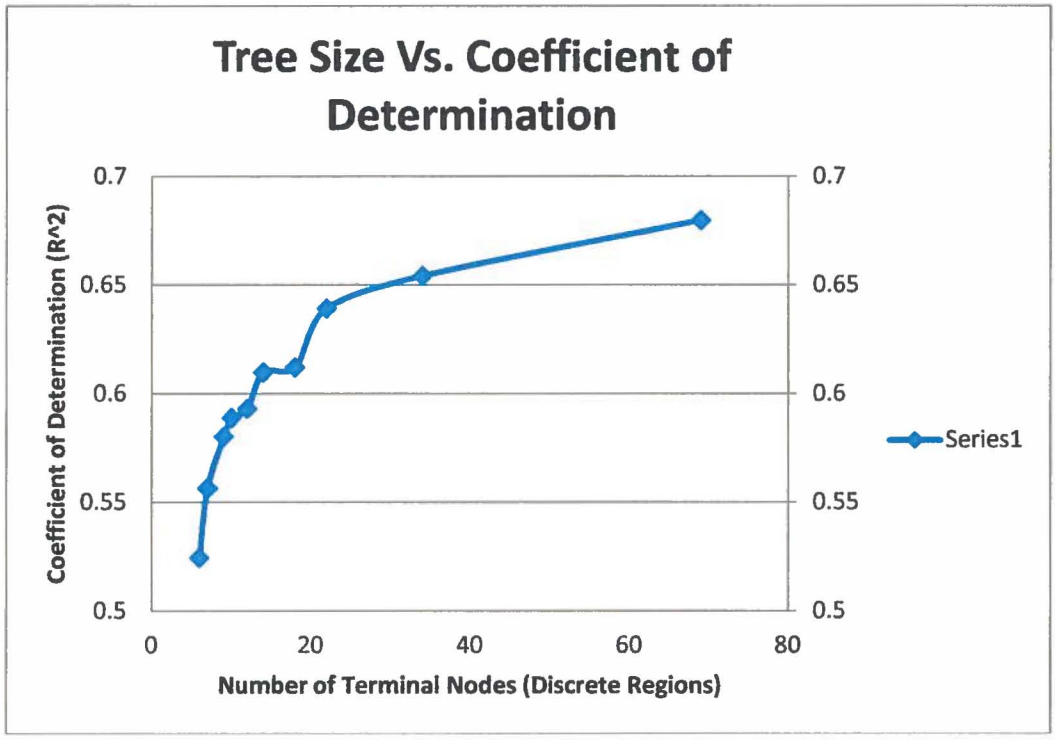


**Figure 16: Number of terminal nodes vs. coeficient of determination for all regression trees.**

Nonetheless, in this study, model fit ranged between $R^2 = 0.52 - 0.68$, depending on tree size, which indicates that LiDAR derived snow depths can be modeled by binary regression trees at the basin scale, in complex mountainous terrain, with reasonable accuracy (Table 2), (Figure 17).

**Table 2: Error statistics for the regression tree snow depth models**

| | Tee1% | Tree2% | Tree3% | Tee4% | Tree5% | Tree6% | Tree7% | Tree8% | Tree9 -10% | Tree1 1-12% |
|---|---|---|---|---|---|---|---|---|---|---|
| # Leaves | 69 | 34 | 22 | 18 | 14 | 12 | 10 | 9 | 7 | 6 |
| $R^2$ | 0.680 | 0.654 | 0.639 | 0.612 | 0.610 | 0.593 | 0.589 | 0.580 | 0.557 | 0.525 |
| μ error (m) | 0.0081 | 0.0083 | 0.0084 | 0.0086 | 0.0086 | 0.0088 | 0.0088 | 0.0089 | 0.0088 | 0.0090 |

| | | | | | | | | | | |
|---|---|---|---|---|---|---|---|---|---|---|
| **Median error** | 0.023 | 0.026 | 0.028 | 0.031 | 0.032 | 0.033 | 0.033 | 0.035 | 0.035 | 0.042 |
| **σ2 of Error** | 0.049 | 0.053 | 0.055 | 0.059 | 0.059 | 0.063 | 0.063 | 0.064 | 0.067 | 0.068 |
| **σ of error** | 0.221 | 0.229 | 0.234 | 0.243 | 0.244 | 0.250 | 0.250 | 0.253 | 0.260 | 0.261 |
| **MSE** | 0.049 | 0.053 | 0.055 | 0.059 | 0.059 | 0.063 | 0.063 | 0.064 | 0.068 | 0.068 |
| **IQ Range** | 0.243 | 0.253 | 0.262 | 0.274 | 0.274 | 0.282 | 0.282 | 0.290 | 0.298 | 0.300 |

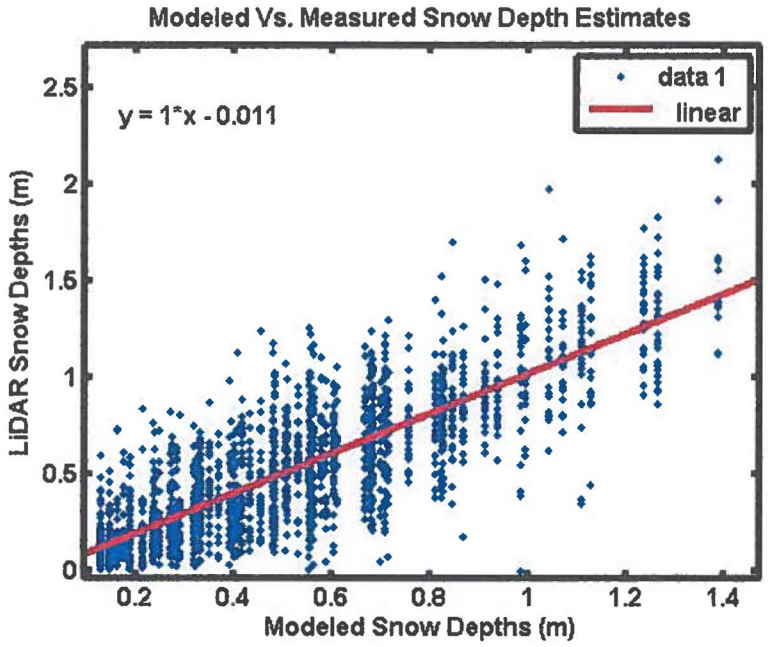


**Figure 17: LiDAR snow depths vs. snow depths modeled using Tree1%.**

Model fit was better than previous studies, which used field-based measurements of snow depth to estimate the spatial distribution of snow in smaller catchments, and thus had far fewer data points to construct regression trees. Balk and Elder (2000) modeled snow depth in a 6.9 $km^2$ catchment using an 18 terminal node tree with an $R^2$ of 0.59. Wintstral et al. (2002) modeled snow depth in a 2.25 $km^2$ basin with an $R^2$ of 0.5. Molotch et al. (2003) used binary regression trees to model snow depths over a 3 month period in the 19.1 $km^2$ Tokopah basin using an average of 9.6 terminal nodes, achieving

an average $R^2$ of 0.44. Erxleben et al. (2002) modeled snow distribution in the forested terrain of the Colorado Rocky Mountains with an average $R^2$ of 0.25. This study was able to account for more variability than previous works because more samples were available and the datasets used to train and validate the regression trees were evenly distributed throughout the snow covered area. Previous studies relied on field campaigns to gather measurements. However, snow travel is inherently difficult and sometimes dangerous, limiting the number of samples that can be gathered in a day, as well as, the locations from which measurements can be safely collected. The snow covered area in the LiDAR dataset contained ~28 million snow depth estimates. The amount of data from which the regression trees were constructed and validated (5 million random samples) was limited only by the available computational resources (Intel Core2 Quad Q9300 processor, 8GB RAM).

Mean squared errors for the entire basin ranged between 4.9 and 6.8 cm (depending on the number of terminal nodes). However, the measurements of dispersion suggest that the variability in the dataset can be a large fraction of the mean snow depth. It may be inferred that the regression trees produce reliable areal estimates of mean snow depth, but should not be used for point estimates.

### 4.3 Optimal Sampling Strategies

Tree1% produced the most accurate estimates of snow distribution, requiring 183 strategically placed samples to be 95% certain that the estimated total snow volume was within 9% of the true snow volume (Figure 18).

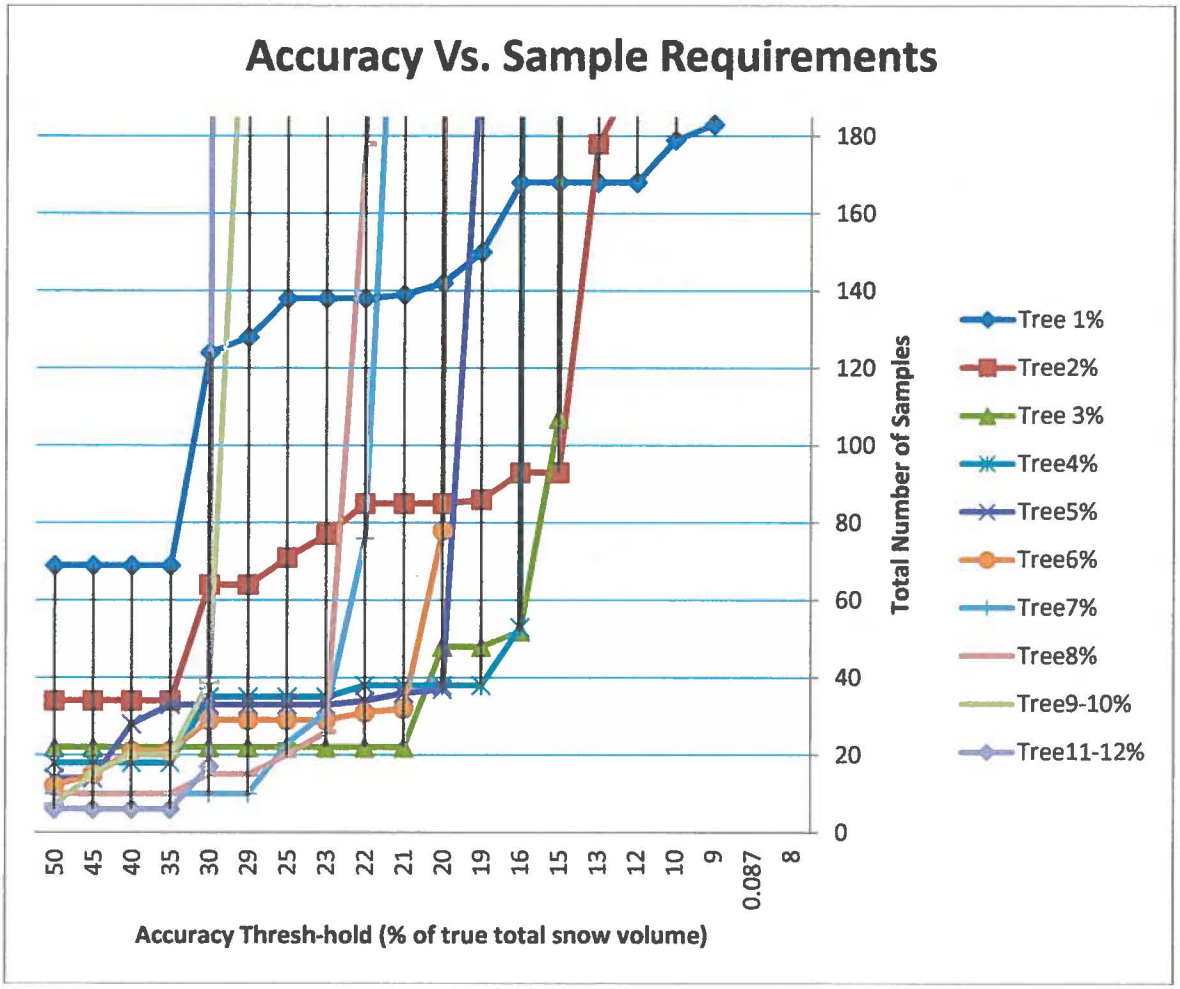


**Figure 18: Sample size vs. accuracy requirements for total basin snow volume estimates.**

Conversely, Tree11-12% (same tree for both minimum leaf constraints) required only six measurements to be 95% certain that estimates were within 35% of the true snow volume. For future surveys, participants should choose the sampling strategy associated with Trees1-12% that balances their project's need for accuracy with their available survey resources.

The optimal tree depended on the accuracy threshold. Each tree had an accuracy limitation that could not be exceeded, regardless of how many samples were added.

There was a direct relationship between the number of terminal nodes and the maximum attainable accuracy. However, with several exceptions, the simplest tree usually required the least samples when the accuracy threshold was within the limits of the tree. The tradeoff between maximum attainable accuracy and minimum sample requirements occurred because as accuracy levels increased, more discrete regions were required to reduce snow-depth variance. However, every additional region required a minimum of one extra measurement, even if the region contributed minimally to the total basin snow volume. Therefore, results suggest that on average, the simplest tree that meets the desired level of accuracy should be used to design the snow survey.

There were two notable exceptions to this trend. Between the 25 and 45% accuracy thresholds, Tree 5% required an average of 5 more samples than Tree4%. Also, Tree9-10% required more samples than Trees 4%, 6%, and 8% over certain threshold intervals. These exceptions occurred because larger minimum leaf constraints forced dissimilar regions to combine, increasing snow depth variance and required sample sizes. This effect was profound when the combined regions contributed significantly to total snow volume and the difference between their mean snow depths was large.

The plot of the mean MAD of snow volume versus sample size shows substantial marginal benefits from ~1-8 samples, then approaches zero asymptotically (Figure 19).

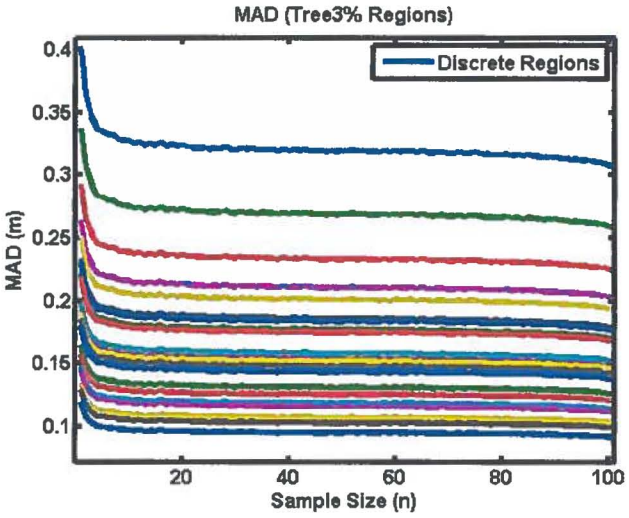


**Figure 19: MAD of mean snow depth estimates vs. sample size.**

Because of this phenomenon, large increases in accuracy were initially achieved with only a few measurements. However, there was a steep decline in marginal benefits, and a total accuracy limitation was rapidly encountered.

A plot of each region's total snow volume versus its assigned sample size shows that, on average, regions that contained more snow were assigned more samples (Figure 20).

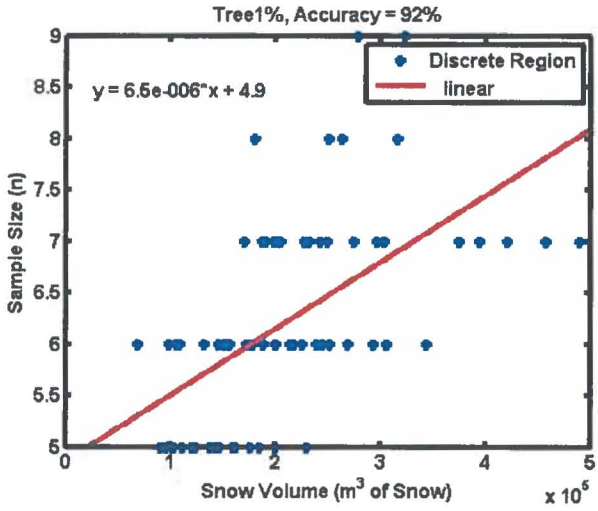

**Figure 20: Sample reguirements for each region as a function of contributing snow volume.**

This occurred for two reasons: 1) total basin snow volume estimates improved more when mean depth estimates for regions with lots of snow improved, and 2) regions with more snow tended to be deeper. Since mean snow depth and variance are positively correlated (Figure 21), the marginal benefits for regions with lots of snow were greater on average (holding sample size constant) than regions with comparatively less snow.

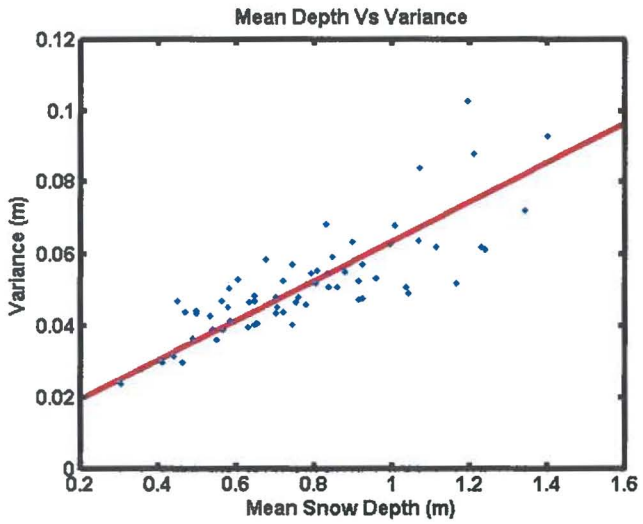


**Figure 21: Variance vs. mean snow depth, using Tree1%.**

Low accuracy thresholds were met by only allocating samples to regions with the most snow and least variability (Figure 21).

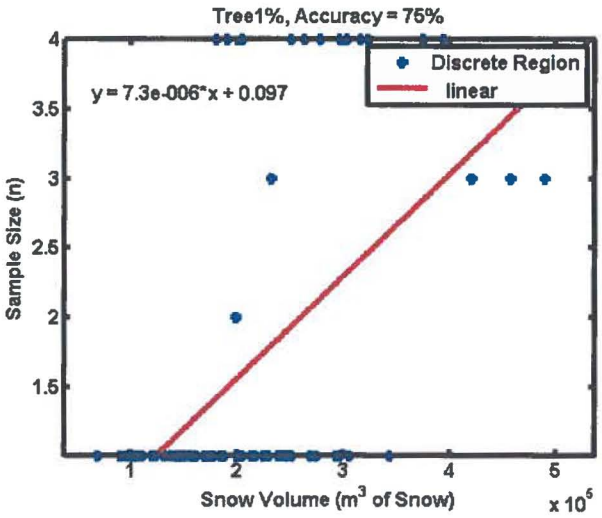


**Figure 22: Sample reguirements for regions in Tree 1% at 75% accuracy level vs. each region's snow volume.**

However, as the accuracy threshold increased and points were added to the most productive regions, their marginal benefits decreased and points were added to regions with less snow and variability (Figure 20).

### 4.4 Validation Snow Surveys

The relative distribution of snow during the LiDAR survey and the two field surveys was comparable (Figures 23a and b).

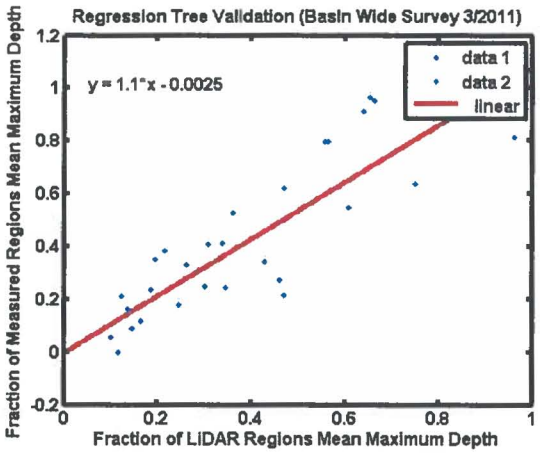


**Figure 23a: Snow distribution during LiDAR survey versus March 3, 2011 survey.**

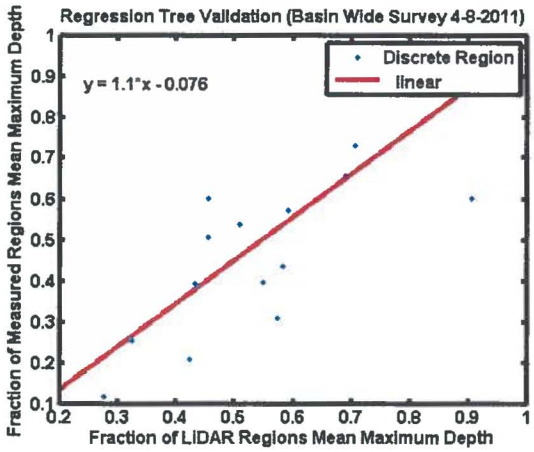


**Figure 23b: Snow distribution during LiDAR survey versus April 8, 2011 survey.**

This suggests that the relative distribution of snow, identified by the regression trees, is temporally persistent, at least during the period of near maximum snow accumulation. It is therefore suggested that the survey strategies previously outlined be adapted to future near peak accumulation dates to make the surveys more efficient and to improve the accuracy of total basin snow volume estimates.

The slope of 1.1 for the linear fit of both plots indicates that the basin-wide surveys tended to overestimate mean snow depths, relative to the distribution during the LiDAR survey. However, during the two surveys, the snow was ripe and air temperatures were well above freezing through-out the afternoon. The melting snow softened the ground, making it difficult to locate the snow-ground boundary, especially during the April survey. Therefore, the snow surveys likely overestimated snow depths.

The box plots of differences between the relative distributions of snow during the field and LiDAR surveys (Figure 24) show nearly unbiased distributions for both dates.

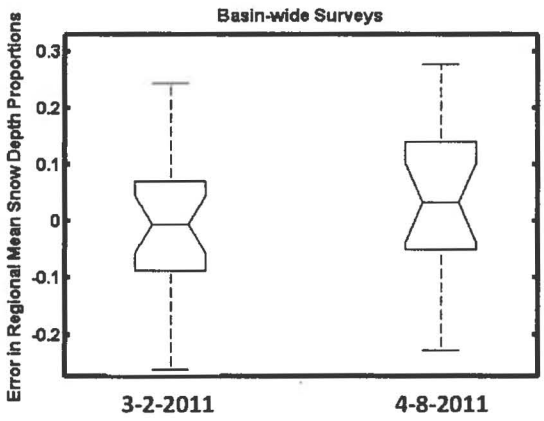


**Figure 24: Boxplots of the difference between relative distribution of regional mean depths. Mean depths for each region were normalized as a fraction of the watershed's maximum mean regional snow depth for the survey date. Error is the difference in each region's proportion of maximum mean snow depth between the LiDAR flight and the field surveys.**

This suggests that during specific temporal intervals, it may be possible to estimate total basin snow volume by estimating regional mean snow depths for unmeasured regions using just the mean depth for a single region (or limited number of regions), and the relative spatial distribution, identified by the regression trees.

### 4.5 Importance of Independent Variables

Although the best predictor variable for a given branch depended on the minimum leaf requirements (Figures 25a-d, Tables 3a-j), results from the variable importance calculations indicate that elevation and total incoming solar radiation were the most important.

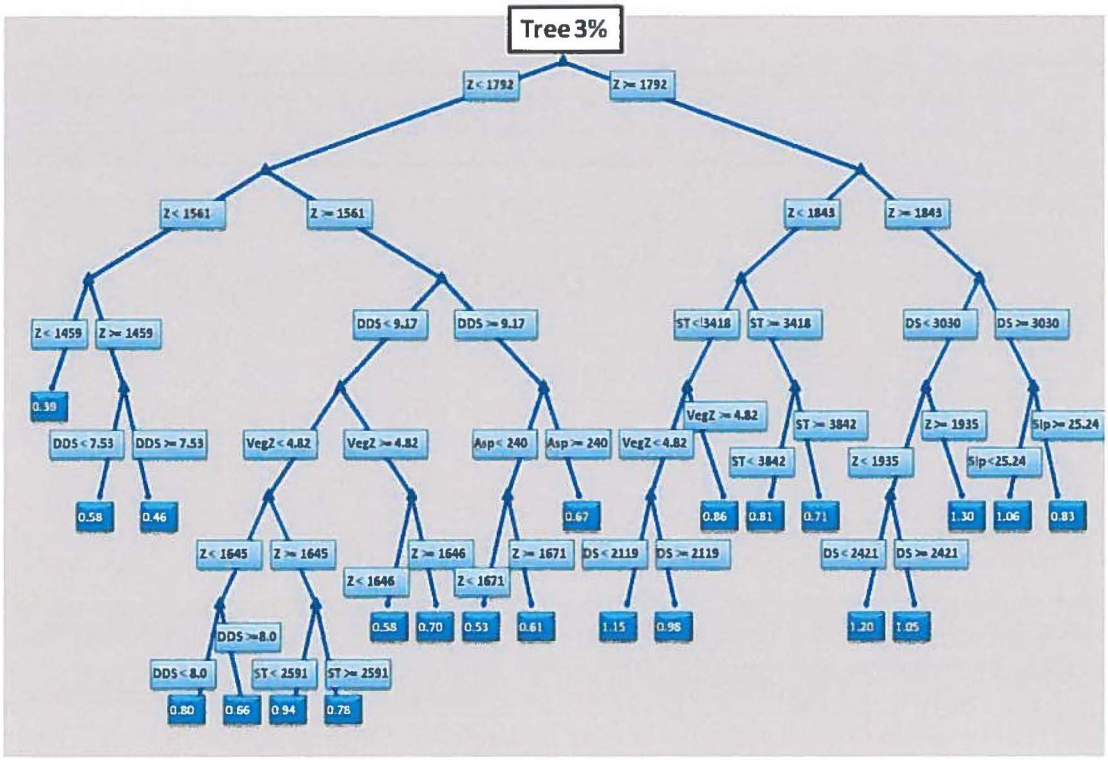


**Figure 25a: Tree 3%. ST= total solar radiation (w/m$^2$), DS = direct solar radiation (w/m$^2$), Z=elevation (m), VegZ= mean vegetation height (m), DDS= duration of direct solar radiation (hrs), Asp=aspect (degrees).**

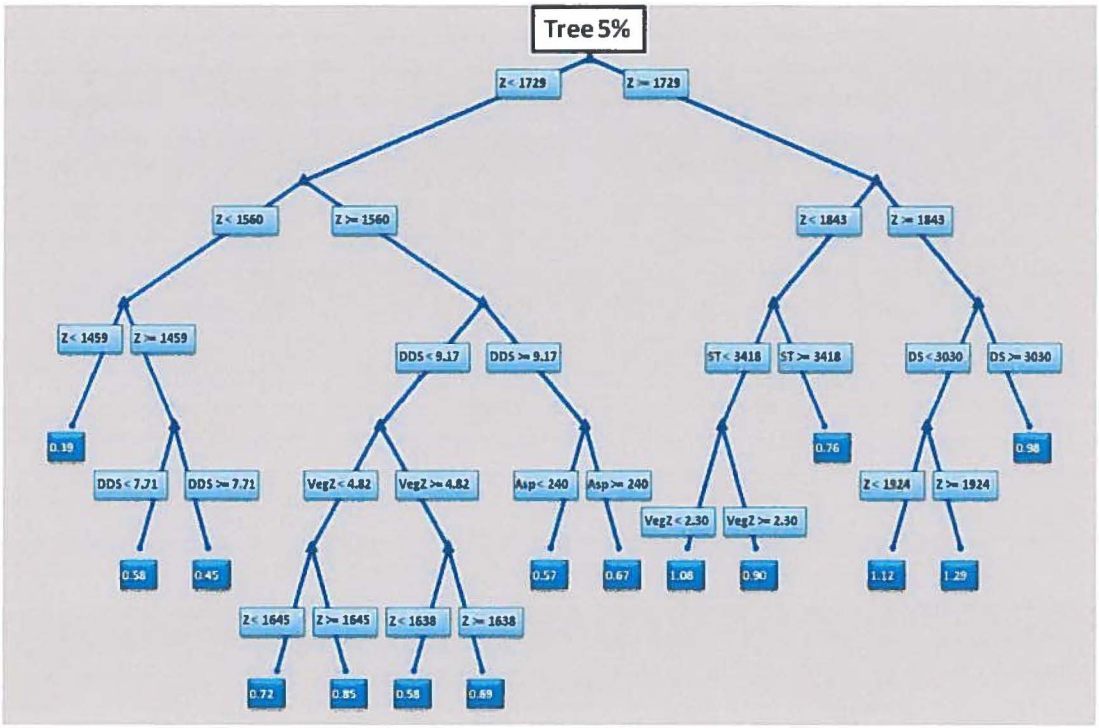


**Figure 25b: Tree 5%**

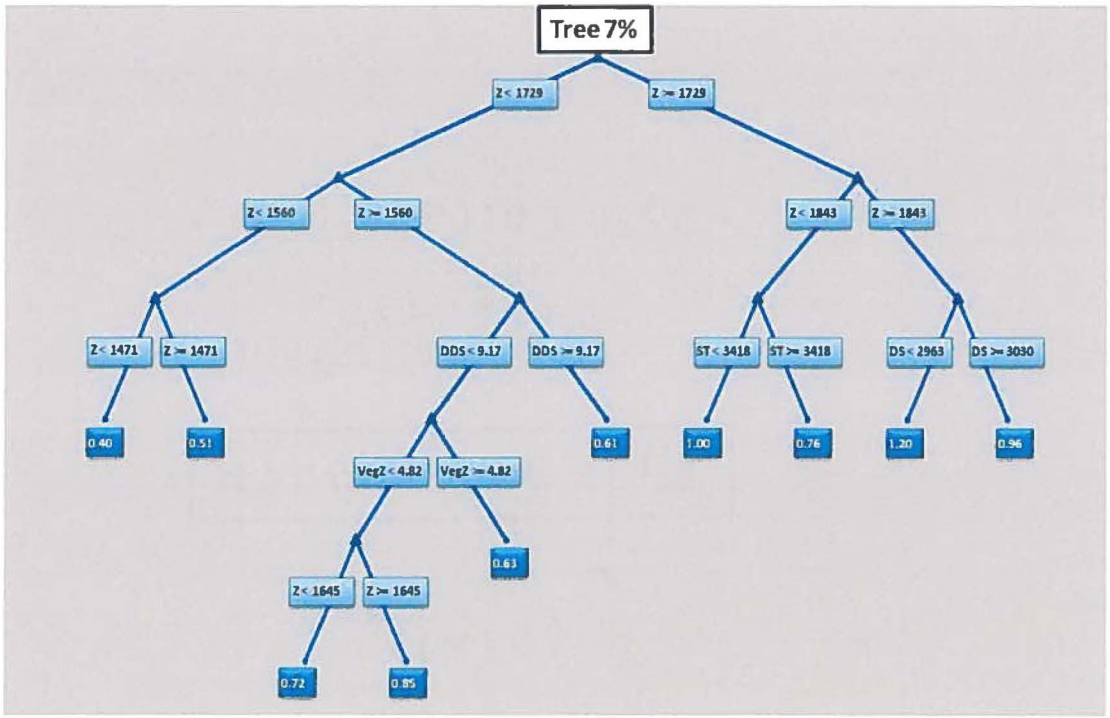


**Figure 25c: Tree 7%**

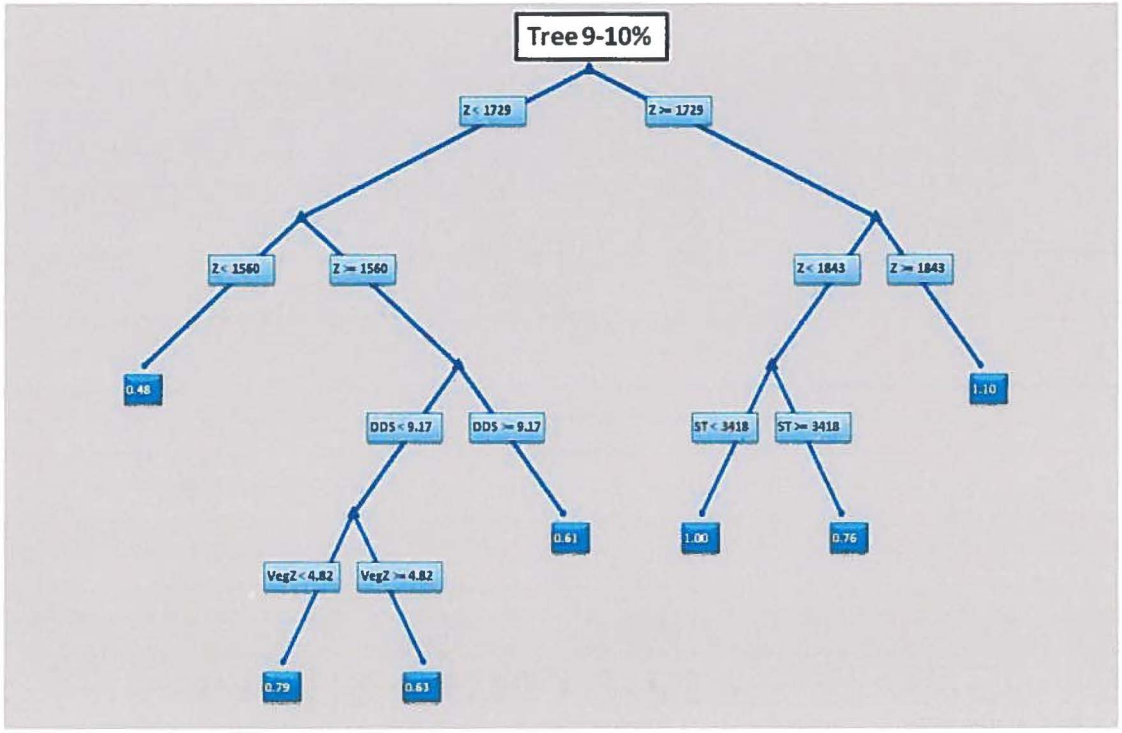


**Figure 25d: Tree 9-10%**

**Tables 3a-j: Independent variable importance, defined as the regression tree's total reduction in the variance of snow depths that can be attributed to each independent variable.**

| Table 3a | Tree 1% | | |
|---|---|---|---|
| **Independent Variable** | **Importance** | **Independent Variable** | **Importance** |
| Elevation | 0.000346929 | Aspect | 4.87E-06 |
| Total Solar | 3.17E-05 | Slope | 3.43E-06 |
| Mean Vegetation Height | 2.82E-05 | Diffuse Solar | 3.38E-06 |
| Direct Solar | 2.78E-05 | Local Roughness | 2.47E-07 |
| Duration of Direct Solar | 1.80E-05 | Northness | 0 |

| Table 3b | Tree 2% | | |
|---|---|---|---|
| **Independent Variable** | **Importance** | **Independent Variable** | **Importance** |
| Elevation | 0.000676054 | Slope | 1.22E-05 |
| Total Solar | 6.35E-05 | Aspect | 6.82E-06 |
| Mean Vegetation Height | 5.81E-05 | Diffuse Solar | 2.68E-06 |
| Direct Solar | 5.49E-05 | Local Roughness | 0 |
| Duration of Direct Solar | 3.49E-05 | Northness | 0 |

| Table 3c | Tree 3% | | |
|---|---|---|---|
| **Independent Variable** | **Importance** | **Independent Variable** | **Importance** |
| Elevation | 0.001040386 | Slope | 1.90E-05 |
| Total Solar | 9.73E-05 | Aspect | 7.80E-06 |
| Direct Solar | 8.04E-05 | Local Roughness | 0 |
| Mean Vegetation Height | 6.43E-05 | Diffuse Solar | 0 |
| Duration of Direct Solar | 5.06E-05 | Northness | 0 |

| Table 3d | Tree 4% | | |
|---|---|---|---|
| **Independent Variable** | **Importance** | **Independent Variable** | **Importance** |
| Elevation | 0.001274169 | Aspect | 9.58E-06 |
| Total Solar | 0.000119487 | Slope | 0 |
| Mean Vegetation Height | 7.82E-05 | Local Roughness | 0 |
| Direct Solar | 7.31E-05 | Diffuse Solar | 0 |
| Duration of Direct Solar | 6.21E-05 | Northness | 0 |

| Table 3e | Tree 5% | | |
|---|---|---|---|
| **Independent Variable** | **Importance** | **Independent Variable** | **Importance** |
| Elevation | 0.001638785 | Aspect | 1.24E-05 |
| Total Solar | 0.000122879 | Slope | 0 |
| Direct Solar | 9.47E-05 | Local Roughness | 0 |
| Mean Vegetation Height | 8.80E-05 | Diffuse Solar | 0 |
| Duration of Direct Solar | 6.41E-05 | Northness | 0 |

| Table 3f | Tree 6% | | |
|---|---|---|---|
| **Independent Variable** | **Importance** | **Independent Variable** | **Importance** |
| Elevation | 0.00189105 | Diffuse Solar | 1.95E-05 |
| Total Solar | 0.00014425 | Aspect | 1.44E-05 |
| Direct Solar | 0.000111179 | Slope | 0 |
| Mean Vegetation Height | 6.74E-05 | Local Roughness | 0 |
| Duration of Direct Solar | 5.47E-05 | Northness | 0 |

| Table 3g | Tree 7% | | |
|---|---|---|---|
| **Independent Variable** | **Importance** | **Independent Variable** | **Importance** |
| Elevation | 0.002288767 | Slope | 0 |
| Total Solar | 0.000174618 | Local Roughness | 0 |
| Direct Solar | 0.00013227 | Diffuse Solar | 0 |
| Mean Vegetation Height | 8.16E-05 | Northness | 0 |
| Duration of Direct Solar | 6.62E-05 | Aspect | 0 |

| Table 3h | Tree 8% | | |
|---|---|---|---|
| **Independent Variable** | **Importance** | **Independent Variable** | **Importance** |
| Elevation | 0.002288301 | Slope | 0 |
| Total Solar | 0.000174618 | Local Roughness | 0 |
| Direct Solar | 0.000122717 | Diffuse Solar | 0 |
| Mean Vegetation Height | 8.16E-05 | Northness | 0 |
| Duration of Direct Solar | 6.62E-05 | Aspect | 0 |

| Table 3i | Tree 9-10% | | |
|---|---|---|---|
| **Independent Variable** | **Importance** | **Independent Variable** | **Importance** |
| Elevation | 0.003237754 | Local Roughness | 0 |
| Total Solar | 0.000255211 | Diffuse Solar | 0 |
| Mean Vegetation Height | 0.000119246 | Direct Solar | 0 |
| Duration of Direct Solar | 9.68E-05 | Northness | 0 |
| Slope | 0 | Aspect | 0 |

| Table 3j | Tree 11-12% | | |
|---|---|---|---|
| **Independent Variable** | **Importance** | **Independent Variable** | **Importance** |
| Elevation | 0.003826436 | Diffuse Solar | 0 |
| Mean Vegetation Height | 0.000140246 | Direct Solar | 0 |
| Duration of Direct Solar | 0.000114399 | Total Solar | 0 |
| Slope | 0 | Northness | 0 |
| Local Roughness | 0 | Aspect | 0 |

These findings agree with other studies (Elder et al., 1995, Molotch et al., 2003). Elevation is reasonable because of its inverse correlation with temperature and positive correlation with total precipitation in the DCEW. Historical records for the catchment indicate that higher elevations receive more precipitation, that more precipitation falls in the form of snow, and that melt rates are slower because of colder temperatures.

All four solar radiation variables were better predictors than the radiation analogs like aspect and northness. The SOLARFLUX algorithm used in this study accounts for the effects of slope, aspect, and topographic shading on solar insolation, creating a more robust estimate. The difference in importance between direct and diffuse solar radiation can be attributed to their relative contribution to total solar radiation in the DCEW, comprising an average of 72% and 28%, respectively, for the dates used in this study.

Although northness was included in the minimum cost sub-tree (for trees1% and 2%), it was removed after pruning. Its lack of importance is contrary to previous findings, which suggested regression tree improvements from the inclusion of northness (Molotch et al., 2003). Additionally, the omission of vegetation roughness, eastness, and all three curvature parameters indicates that they were not primary controls on the spatial distribution of snow in the DCEW at the scales examined in this study.

# CHAPTER 5: CONCLUSION

This research demonstrates that binary regression trees can be used with Airborne LiDAR estimates of snow depth to divide snow covered areas into regions of similar snow distribution and construct objective sampling strategies for extents that would otherwise be too large to thoroughly sample. Since the relative distribution of snow was similar on all three survey dates, the sampling strategies outlined in this paper are recommended when snow accumulation is near peak. However, new snow surveys should be performed throughout the accumulation and melt season to estimate the within season temporal variability in the relative distribution of snow depth.

These sampling strategies should improve the accuracy of total basin snow volume estimates and increase the efficiency of snow surveys in the DCEW because they minimize the number of samples required to meet each accuracy threshold, efficiently distribute point estimates through space, balance accuracy requirements with survey resources, and allow sample collection from easily accessible locations. The high resolution LiDAR dataset made it possible to design optimal sampling strategies and indentify the topographic controls on the spatial distribution of snow in a manner that was not feasible with surveyed measurements. Using the marginal benefits to define the spatial distribution of sample densities was important because it decreased total sample requirements and directed the use of limited survey resources towards the most important regions.

In locations where the relative spatial distribution of snow persists during specific periods, it may be feasible to estimate snow distribution in unmeasured regions as a function of the mean depths at easily measured locations, provided the relative spatial distribution is known. In some locations, this could expand the spatial extent and improve the accuracy of snow estimates. This approach would also be helpful in regions that are difficult to access, dangerous to sample, or when sample requirements exceed available resources.

Future research on the relative spatial and temporal distribution of snow density could improve SWE estimates. Jonas et al., (2009) used calibrated depth-density relationships to estimate snow density and calculate SWE from depth measurements alone. Their model's uncertainty was of the same order of magnitude as the variability of repeated density measurements at one site. Therefore, the combination of the two strategies could feasibly lead to further improvements in survey efficiency and total basin SWE estimates.

LiDAR's accuracy for gridded snow depth estimates ± ~20 cm ($\sigma$ from Table 1) limits the viability of this technique in shallow, patchy snowpacks because the noise in the LiDAR data is on par with the snow depths. The proposed method will be most beneficial in large, inaccessible regions with deep snow. This is because only small, easily accessible, safe subsections of each region need to be sampled to determine the snow distribution for large regions, and errors in LiDAR depth estimates will be small compared to the actual snow depths.

**Recommended Steps for Future Surveys**

1) Decide which combination of discrete regions to use (Figure 18). More regions = more accurate but requires more sample resources (people, depth probes, SWE tubes).

Note: Trees 2, 4, 8, 10, 12, and 15% have been converted into maps (LiDAR_DEM/Discrete_Snow_Regions). All other regression trees need to be converted into maps before they can be used for surveys.

2) Import the file of discrete regions into ArcMap and symbolize each region with a different color.
3) Create a new points class shapefile (using a projection of NAD83, Zone 11North) and select easily accessible locations within each of the discrete regions. Since the accuracy of hand-held GPS units is usually around 5-20 meters, select sample locations that are well inside of the discrete snow regions.
4) Record the x and y positions, as well as the discrete region number and enter these values on the field survey sheets to be filled in by surveyors.
5) Take 8-12 depth measurements within a 5 meter radius in each discrete region.
   Note: After about 10 measurements, the value of an additional point decreases rapidly (Figure 19).
6) Average the depth and density measurements for each discrete region and multiply to get average SWE for each region.
7) Open ArcMap, import each of the discrete regions' files (every cell should = 1). Open raster calculator (in spatial analyst). Multiply each region by its average SWE value.

8) Open the Mosaic to New Raster tool and select each of the files created in Step 7 as input rasters. The result is a SWE map of the entire watershed.

WORKS CITED

Aishlin, P., and McNamara, J.P., 2011. Bedrock infiltration and mountain block recharge accounting using chloride mass balance. Hydrological Processes DOI: 10.1002/hyp.7950.

Anderton SP. 2000. An analysis of spatial variability in snow processes in a high mountain catchment. PhD thesis, School of Engineering, University of Durham.

Bales, R. (1995). *Recent progress in snow hydrology.* University of Arizona, Department of Hydrology and Water Resources. Tucson, USA: U.S. Natl. Rep. Int. Union Geol. Geophys.

Balk B, Elder K. (2000). Combining binary decision tree and geostatistical methods to estimate snow distribution in a mountain watershed. *Water Resources Research* , *36* (1), 13-26.

Bloschl G, K. R. (1992). An analysis of snow cover patterns in a small alpine catchment. *Hydrological Processes* , 99–109.

Breiman, L., Friedman, J.H., Olshen, R., Stone, C., 1984, Classification and Regression Trees: Belmont California, Wadsworth International Group, 358.

Chambers J., T. Hastie (Eds.), *Statistical Models in S*, Wadsworth, Belmont, Calif., 1993.

Cline, D. B. (1998). Estimating the spatial distribution of snow in mountain basins using remote sensing and energy balance modeling. *Water Resources Research , 34* (5), 1275-1285.

Deems, J. (2006). LiDAR measurement of snow depth: Accuracy and error sources. (J. Gleason, Ed.) *Proceedings of ISSW* , 330-338.

Deems, J. S., S. R. Fassnacht, and K. J. Elder. (2006). Fractal distribution of snow depth from LiDAR data. *Journal of Hydrometeorology 7(2): 285-297.*

Doesken, N.J., and A. Judson, The Snow Booklet: A Guide to the Science, Climatology, and Measurement of Snow in the United States, Dep. of Atmos. Sci, Colo. State Univ.. Fort Collins, 1996.

Elder K, Dozier J, Michaelsen J. (1991). Snow accumulation and distribution in an alpine watershed. *Water Resources Research , 27*, 1541-1552.

Elder, K., J. Michaelsen, and J. Dozier (1995), Small basin modeling os snow water equivalence using binary regression tree methods, in Biogeochemistry of Seasonally Snow-Covered Catchments, edited by K.A. Tonnessen et al., IAHS Publ., 228, 129-139,.

Elder, K. J. (2006). Verification of lidar data for snow depth. *in preparation* .

Engineers, U. A. (1998). Runoff from snowmelt. *Engineer Manua lNo. 1110-2-1406* , 142.

Erxleben J, Elder K, Davis RE. 2002. Comparison of spatial interpolation methods for estimating snow distribution in the Colorado Rocky Mountains. *Hydrol. Process.*, 16: 3627-3649.

Hopkinson, C., Sitar, M., Chasmer, L.E., Treitz, P. (2004). Mapping Snowpack Depth Beneath Forest Canopies Using Airborne LiDAR. *Photogrammetric Engineering and Remote Sensing,* 70 (3) pp. 323-330

Hosang J, D. K. (1991). Evaluation of a water equivalent of snow cover map in a small catchment area using a geostatistical approach. *Hydrological Processes , 5*, 283–290.

Jonas, T., Marty, C., Magnusson, J. (2009) Estimating the snow water equivalent from snow depth measurements in the Swiss Alps. *Journal of Hydrology*, 378, 161-167.

Jones, H.G., 1999: The ecology of snow covered systems: a brief overview of nutrient cycling and life in the cold. *Hydrological Processes*, 13, 2135-2147.

Streutker, D. and Glenn, N., 2006. LiDAR measurement of sagebrush steppe vegetation heights. *Remote Sensing of Environment*, 102, 135-145.

Molotch NP., Bales RC., Colee, MT., Dozier J, (2003). Optimization of Binary Regression Tree Models for Estimating the Spatial Distribution of Snow Water Equivalent in an Alpine Basin.

Tarboton, D. G. (1991). Preliminary comparisons of snowmelt models for erosion prediction. *Proceeding of Western Snow Conference*, *59*, pp. 79-90.

Winstral A, Elder K, Davis RE. 2002. Spatial snow modeling of wind-redistributed snow using terrain-based parameters. Journal of Hydrometeorology 3: 524-538.

Wolford, R. A. (1996). Development of hydrochemical models for seasonally snow-covered alpine watersheds: Application to Emerald Lake watershed, Sierra Nevada, California. *Water Resour. Res.* , 32(4), 1061-1074.